Master's Thesis

# Segmented Differential Power Processing Structure for Large-Scale Photovoltaic Systems

Hoejeong Jeong

Department of Electrical Engineering

Graduate School of UNIST

2019

# Segmented Differential Power Processing Structure for Large-Scale Photovoltaic Systems

Hoejeong Jeong

Department of Electrical Engineering

Graduate School of UNIST

# Segmented Differential Power Processing Structure for Large-Scale Photovoltaic Systems

A thesis
submitted to the Graduate School of UNIST
in partial fulfillment of the
requirements for the degree of
Master of Science

Hoejeong Jeong

11. 28. 2018
Approved by

Advisor
Katherine Ann Kim

# Segmented Differential Power Processing Structure for Large-Scale Photovoltaic Systems

Hoejeong Jeong

This certifies that the thesis of Hoejeong Jeong is approved.

11. 28. 2018

Katherine Ann Kim

Jee-Hoon Jung

Jun Moon

Jun Moon

# Abstract

Renewable energy, like photovoltaic (PV) energy, has recently become popular as power consumption and environmental problems have become bigger social issues. However, the mismatch among the series-connected PV panels decreases the DC voltage and output power at the maximum power point(MPP). To solve this problem, full power processing (FPP) converters are used for finding the MPP of each PV. This FPP converter processes the full amount of rated power, which has a high-power rating and induces power losses. Instead, the differential power processing (DPP) converter processes a small amount of rated power, which can achieve MPP operation with smaller converter power ratings and lower cost.

However, DPP converters in large-scale systems have challenges of complicated wire connections and high voltage ratings. To overcome these scalability problems, the segmented DPP structure is introduced, and the control algorithm and converter development are discussed. Both voltage balancing and maximum power point tracking (MPPT) algorithm are used to effectively control the system operation. With this algorithm, the segmented DPP system was evaluated through the Matlab/Simulink simulation. Also, the segmented DPP converter, which consists of bidirectional DC-DC converters, was designed for a prototype module. The segmented DPP system successfully controls the current of each PV panel to reach its MPP in various experimental conditions. The results show a 14.1% system efficiency increment compared to the series-connected system under 28.6% mismatch, which has 99.8% tracking efficiency and 95.73% module efficiency. Under 42.9% mismatch, the system efficiency is increased by 14.8% Also, when the four PVs are all mismatched, system efficiency is increased by 21.4% compare to the series-connected system.

# Contents

# List of Figures

# List of Tables

# I Introduction

Solar energy is the most permanent and abundant renewable energy on the earth. However, 80% of the present energy in worldwide is from non-renewable energy like fossil fuels and nuclear energy. These kinds of energy are decreasing gradually and causing the envirnmental problems like pollution. To address this problem, renewable energy, which has significantly lower envirnmental impact, becomes popular not only at the technical level but also at the political level. For example, the Europe Union has a policy to replace 20% of energy consumption with 2020 [1, 2]. Figure 1.1 shows an estimate of the energy demand and resource, breakdown in the future to the years 2050 and 2100 [3]. As shown in this analysis, non-renewable energy will be less that 15% of the total energy, while solar energy will generate 70% of the total power. Among the ways to capture solar energy, photovoltaic cells can be used to directly convert solar energy to electrical energy, which is a more effective way to collect solar energy than indirect conversion like solar heat. Figure 1.2 shows the potential of photovoltaic power in the world and Korea [4].

In implementation, PV cells are usually connected in series to compose one PV panel, due to the limited DC voltage of one cell. To connect PV panels to the grid system, PV panels are connected in series, then an inverter transfers the PV power to the grid power.

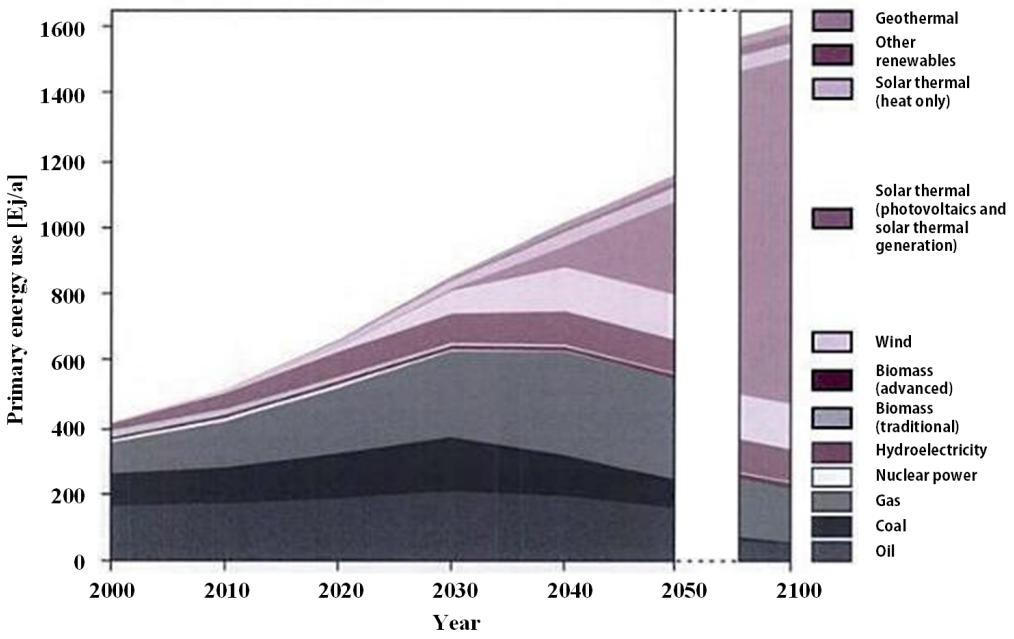


Figure 1.1: Transforming the global energy to 2100 [3]

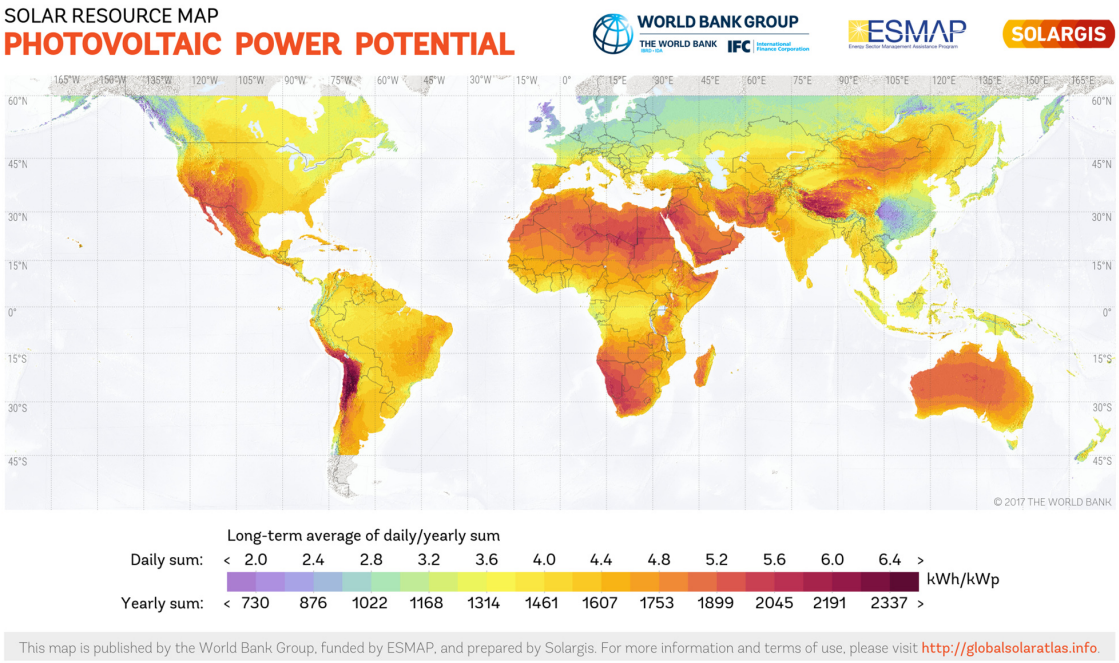


(a)


(b)

Figure 1.2: Photovoltaic power potential in (a) the world and (b) Korea [4]

## 1.1 Conventional PV Systems

Traditionally, PV panels are connected in series, which are then connected to a central converter. This converter controls the PV panels to operate at its maximum power point (MPP) and transfers power from the PV panels to the load. However, this series-connected system cannot generate the maximum power when there is the mismatch among the PV panels [5]. This mismatch can occur because of partial shading, temperature change, degradation or installation at different angles [6,7]. For example, as shown in Figure 1.3a, when there is no mismatch among the PV panels, the current at maximum power point of each panel is the same. However, when mismatch occurs, like in Figure 1.3b, the current at the MPP becomes different from each other. In the series-connected system, the PV currents should flow at the same value through the panels, so that MPP operation for all PVs cannot be achieved in the mismatched panel condition. Furthermore, as shown in Figure 1.3c, if the mismatch among the panel becomes more severe, the PV could be dissipating power. Therefore, in a conventional series-connected system, the bypass diode is connected with PV panels in parallel, which can prevent operating the panels in reverse bias.

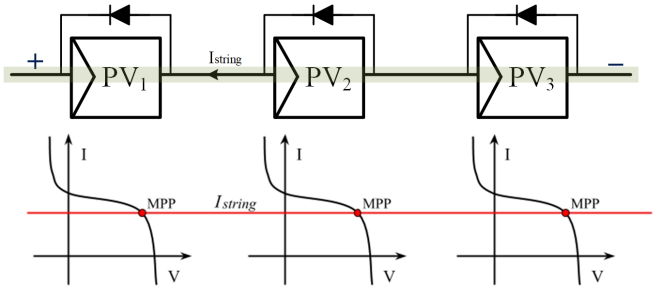


(a) No mismatch among the PV panels

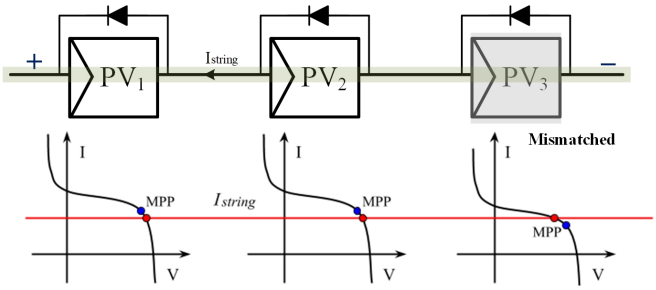


(b) Mismatch among the PV panels

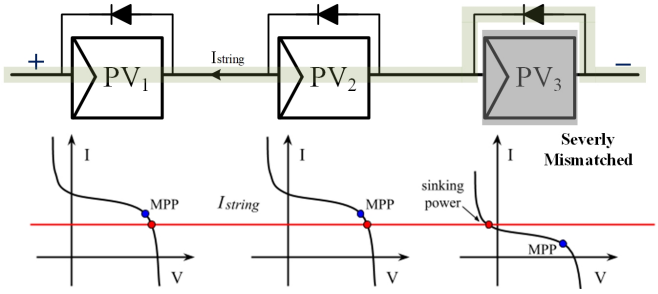


(c) Severe mismatch among the PV panels

Figure 1.3: I-V curve for the series-connected system

To overcome these problems in series-connected systems, dc optimizers or micro inverter, which is known as the full power processing (FPP) systems, are widely used as shown in Figure 1.4 [8–10]. These FPP converters are usually connected to each PV panel and control the PV power individually [11, 12]. Due to the individual control, the PV panels can produce each near-maximum power. However, the converters process the full amount of PV power, so which causes additional power losses. The FPP system efficiency from PV to output is the same as the efficiency of the FPP converters.

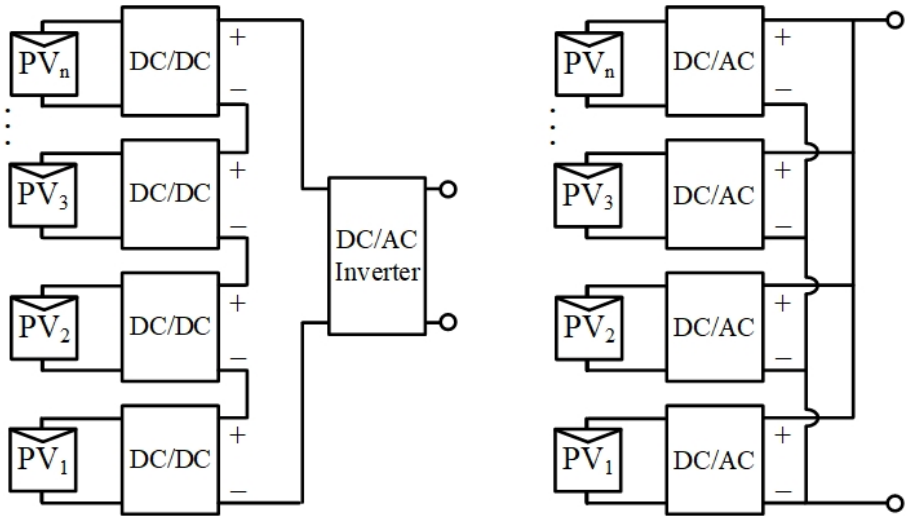


(a) DC optimizer PV system (b) Micro inverter PV system

Figure 1.4: Full power processing system

## 1.2 Differential Power Processing Systems

Recently, differential power processing (DPP) systems have been studied to achieve high efficiency under partial shading and mismatched conditions. These DPP converters are also connected with each PV panel like FPP converters, but the architecture is fundamentally different. Only when the PV panels are mismatched, then the DPP converter transfers a small amount of power to maintain MPP [13–15]. In other words, DPP converter processes a smaller amount of power compared with the FPP system. Figure 1.5 shows the main current flow of the FPP and DPP system. As shown, in the FPP system, the main power flows through the FPP converters, which process the full amount PV power. Conversely, in the DPP system, the main power flows through the PV panels and DPP converter processes a small amount of power. For this reason, the power rating of the DPP converter is lower than the FPP converter, such that the converter loss and cost are lower.

An example of a DPP converter structure, referred to as PV-to-Bus DPP, is shown in Figure 1.6 [16–18]. In PV-to-bus DPP system, the output of the DPP converters are connected to the PV string voltage [14, 19]. This means that the large number of PV panels makes higher voltage rating of each DPP converter. For example, when there are $m$ PVs for a system, the DPP converters should be designed to step up $m$ times to the PV voltage. For smaller numbers of modules, this problem is tractable but scaling up the number of PV panels is more difficult. Also, the physical wire connections of a PV-

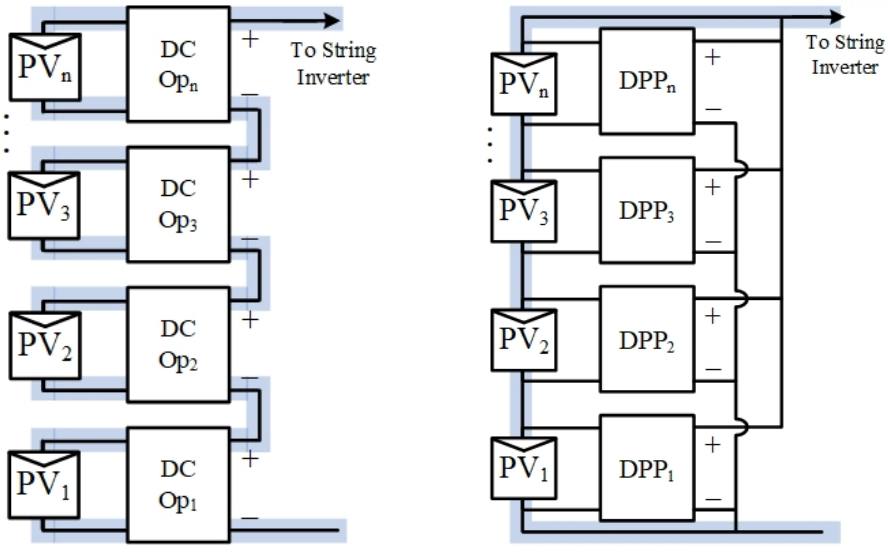


(a) FPP system (b) DPP system

Figure 1.5: Main current flow of the FPP and DPP system

to-Bus DPP system are complicated and require many connections. Further, in order to scale up the number of PV panels, the DPP converter design and wiring should be changed, which is cost and labor intensive. Therefore, although DPP systems have the advantage of lower system losses, they are difficult to design for large-scale PV systems because they require very high output voltage rating and complex wire connections [20]. For these reasons, full-scale DPP systems have not been commercially viable.

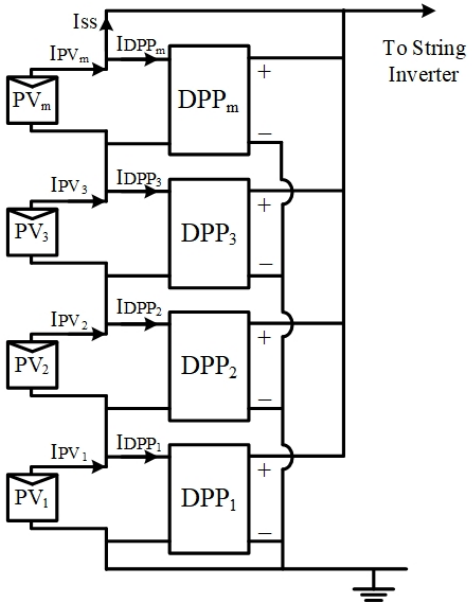


Figure 1.6: Differential power processing system (PV-to-bus)

## 1.3 Goals and Organization

This thesis introduces the structure and algorithm of the segmented DPP system solving the difficulties of the existing DPP system, which is hard to install for large scale PV systems. Also, simulation and experimental testing was conducted to verify this system.

In Section II, the structure of the segmented DPP system and the advantages compared to the existing DPP system are described. Section III explains the algorithm of the segmented DPP system, and suggests an effective control algorithm, which is considered with sensor requirements. In Section IV, a bidirectional flyback converter design for the DPP converter and the system prototype module are described. The experimental results with this prototype and algorithm was presented in Section V. The system was verified under the indoor and outdoor conditions, and the updated prototype and algorithm is described in Section VI. With this updated prototype, the performance of the segmented DPP system was tested, which can find the MPP in various experimental conditions. The last section concludes the thesis and suggest the potential future work for this system.

# II Segmented DPP Systems

If the DPP converter is applied to a system that is frequently exposed to shade on the PV panel, such as building integrated photovoltaic (BIPV), it can generate maximum power at higher efficiency than a typical series connection or FPP system. In addition, the DPP system can be effectively used when the characteristics of the PV panel are different from the installation stage, for example, putting the colored panel on the PV panel, as shown in Figure 2.1 [21]. However, as mentioned in Section I, large-scale DPP systems like BIPVs have problems on the practical installations due to the complexity of wiring and the high step-up ratio of the converter. To solve these problems of converter design and system installation, a *segmented DPP* system is proposed. Also, the structure and advantages of the segmented DPP system will be described in this section.

Figure 2.1: Building integrated photovoltaic (BIPV) with color [21]

## 2.1 Structure of Segmented DPP System

In segmented DPP systems, each segmented DPP module consists of $n$ DPP converters connected to $n$ PV panels and one unit converter. Figure 2.2a shows an example of PV system applied unit DPP system when $n = 4$. The input of each DPP converter is connected to one PV panel and the output of each DPP converter is connected in parallel to the input of the unit converter. The output of the unit converter is connected over the $n$ PV panels strung in series. The DPP converter is a bidirectional flyback converter and the unit converter is a boost that can also operate bidirectionally. Figure 2.2b shows another structure of the segmented DPP module, which consists of $n$ DPP converters with $n$ PV panels. The difference with the previous system is the absence of the unit converter. Due to this difference, the converter loss and cost decrease, and the control complexity of the algorithm can be reduced. However, the DPP converter of this structure has a higher voltage stress, which is trade off compared to the unit converter.

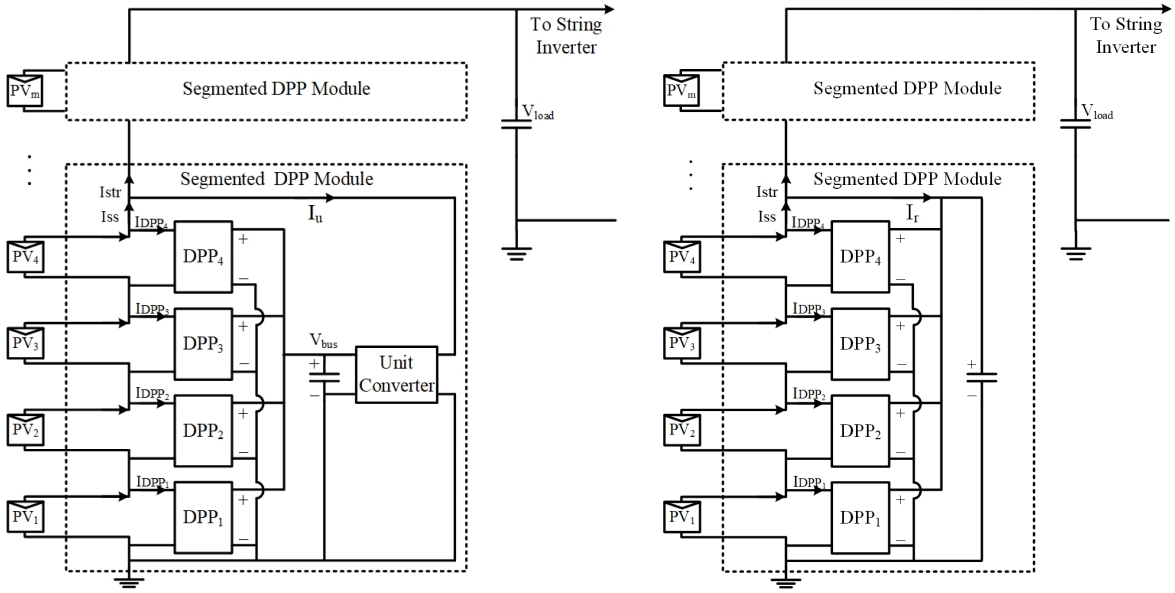


(a) (b)

Figure 2.2: Segmented DPP system (a) with unit converter and (b) without unit converter

In the structure of the segmented DPP system, because the output of the DPP converter is not directly connected to the string inverter, the number of segmented DPP modules is flexible. In other words, the same segmented DPP module design can be applied to shorter or longer strings of PV panels. One design goal of this approach is to use standard PV panel wire cables to connect to the segmented DPP module, which generally limits the number of PV connections to $n < 9$. There is a basic trade-off between the number of panel connected in one segmented DPP module and system performance. Lower $n$ decreases the segmented DPP converter's voltage boost ratio and reduces the number of connections to each module, but it also reduces the output performance. The output performance is related to the number of panels that can exchange power; more converters means that the PV panels can more easily find balance among the various panels, while fewer panels means that the converters are more likely to reach their operating limit.

## 2.2 Advantages of Segmented DPP System

With this segmented DPP structure, there are advantages compared with the existing DPP system. First, this segmented DPP system structure can reduce the voltage rating of DPP converters. Figure 2.3a shows the existing DPP system and the segmented DPP system, which has total $m$ PV panels in system and $n$ PV panels in one module. As shown in the figure, the existing DPP converter should boost up the voltage $m$ times. However, with the segmented DPP converter, the voltage boosting ratio is up to only $n$ times, as shown in Figure 2.3c. Furthermore, in the structure of Figure 2.3b, which includes the unit converter, the secondary-side voltage rating of the DPP converter is only the unit bus voltage. For example, let $m$ be 12, $n$ be 4, and the open-circuit PV voltage be 10 V and the unit bus voltage be 25 V. Then, the secondary-side voltage of the existing DPP converter is about 120 V ($V_{oc} \times m$), while the

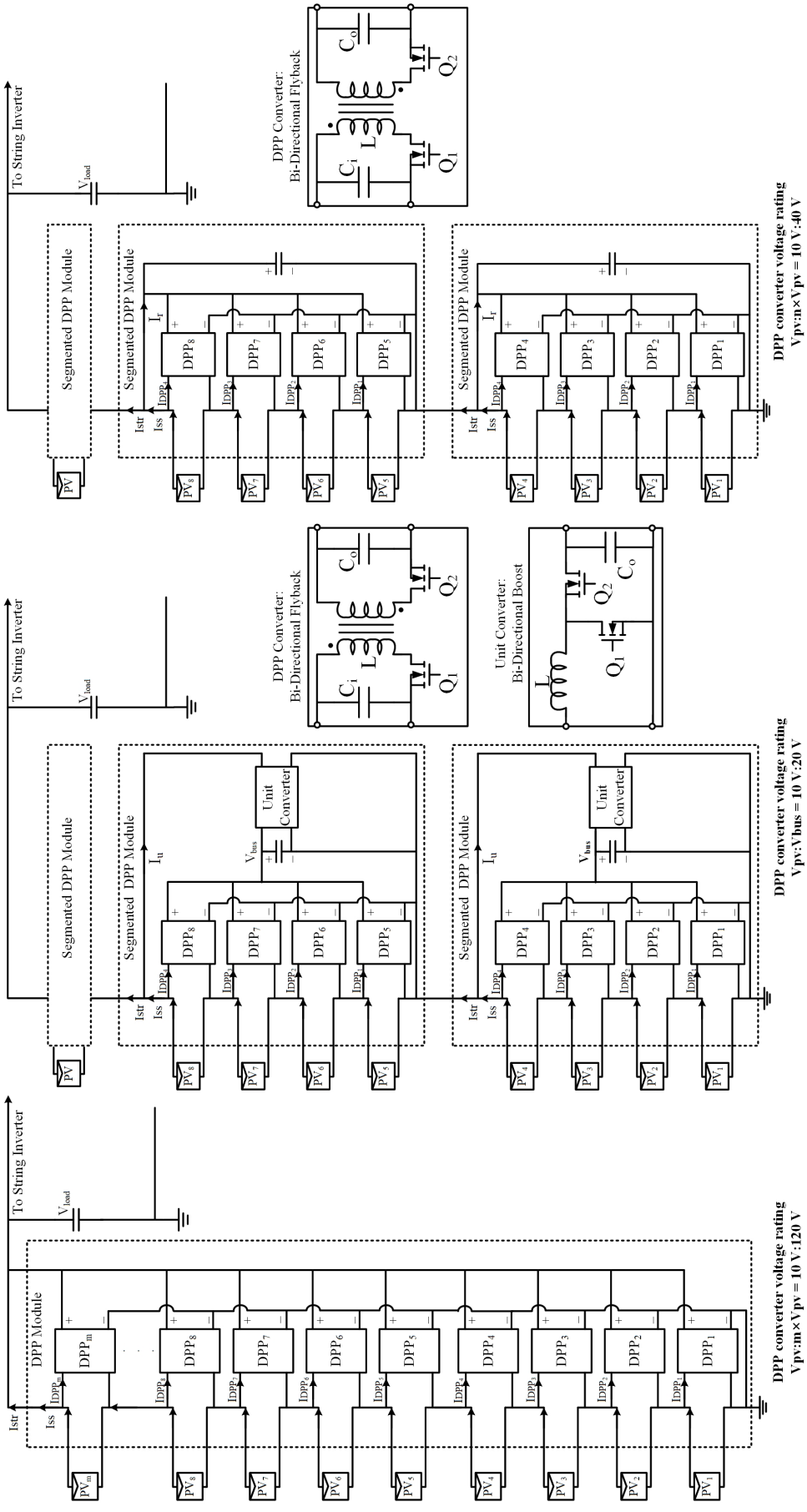


(a) Existing DPP system (b) Segmented DPP system with unit converter (c) Segmented DPP system without unit converter

Figure 2.3: Comparing the existing DPP system and segmented DPP systems

segmented DPP converter is 40 V ($V_{oc} \times n$). Also, with the unit converter, the voltage rating of the DPP converter becomes 20 V, which is a value set by the designer. Therefore, this structure enables the DPP converters to be designed with lower voltage stresses and lower cost.

Also, with the existing DPP system, then the converter and controller must be redesigned to modify the number of the PVs. However, with the proposed segmented DPP system structures, it is much easier to add or modify the number of PV panels and does not require redesigning the DPP converters. The wire connection diagram of the proposed segmented DPP system is shown in Figure 2.4, using standard wire lengths and straight-forward installation. As a result, PV power generation systems with the segmented DPP modules have a higher system power efficiency than traditional full power processing systems and can overcome the drawbacks of existing DPP systems.

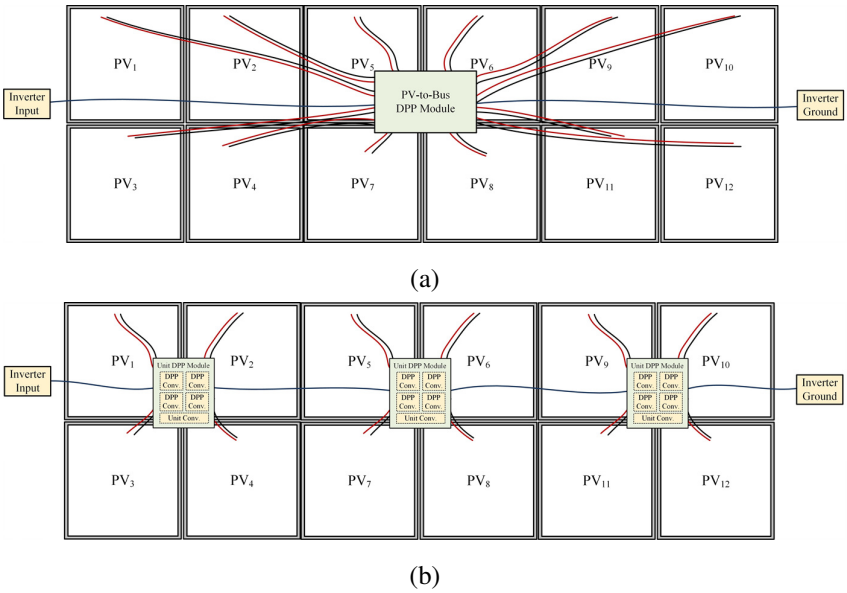


Figure 2.4: The wire connection of (a) existing DPP system and (b) segmented DPP system

# III System Control Evaluation with Simulation

## 3.1 System Algorithm

The goal of the segmented DPP algorithm is for each DPP converter to operate the PVs at their real MPP, while reducing the implementation costs. There are two modes in the segmented DPP system control algorithm: voltage balancing and MPPT algorithm. The bidirectional dc-dc converter which is used as the DPP converter can conduct this algorithm by controlling the primary-side current of the converter. If the reference current is set as a value, the PI controller regulates the primary-side current to the reference current. When the reference current is positive, then the power of the converter flows in the forward direction, and when the reference current is negative, the power flows in the reverse direction. Also, when the reference current is zero, the converter turns off.

### 3.1.1 Voltage Balancing

The voltage balancing algorithm controls PV voltages within a certain range and Figure 3.1 shows the flowchart of voltage balancing. When the current of the PV increases, the voltage of the PV decreases. By this characteristic of the PV panel, we can implement the voltage balancing algorithm. If the measured voltages of the panels are not in a certain range, the index of the PV with the highest voltage is identified, and the reference current of that index is increased by a set amount ($\Delta I$). The index of the PV with the lowest voltage is also identified and the reference current is increased by the same amount to increase the voltage of that PV. Even in most shaded PV cases, the PV voltage at maximum power point is similar to the PV voltage when it is not shaded. For this reason, some systems use only a voltage balancing algorithm to ensure the PV panels are in near maximum power [22, 23]. However, these points are not the real MPP in each PV panel. Therefore, to reach the real MPP, the segmented DPP system additionally uses a MPPT algorithm.

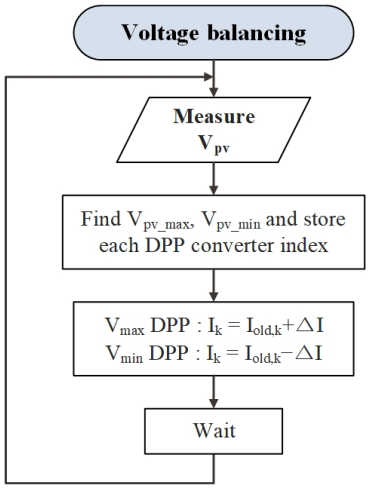


Figure 3.1: Voltage balancing algorithm for the segmented DPP module

### 3.1.2 Maximum Power Point Tracking

After the voltage balancing algorithm gathers the PV voltages within a certain range, each PV panel operates near MPP. Then, the MPPT algorithm is used to find the individual real MPP. The MPPT control algorithm is similar to the perturb and observe (P&O) algorithm [24, 25]. Figure 3.2 shows the flowchart of the MPPT for the segmented DPP system. First, it measures the voltage and current of the PV panel to measure the power of each PV. Then, it changes the primary-side reference current of the DPP converter and compares the total power with the previous total power. If this change makes the total power increase, then the system maintains the new reference current, and if this change makes the total power decrease, then the reference current goes back to the previous value and changes the direction of increment. The operation of the segmented DPP converters are highly coupled with each other, so it is difficult to change all the reference currents at once. Therefore, the reference current of each converter changes in a sequence. For example, when a module consists of four DPP converters, the first converter will execute the algorithm and then the second converter will execute the algorithm. Also, when the fourth converter finishes the algorithm, then the sequence returns to the first converter.

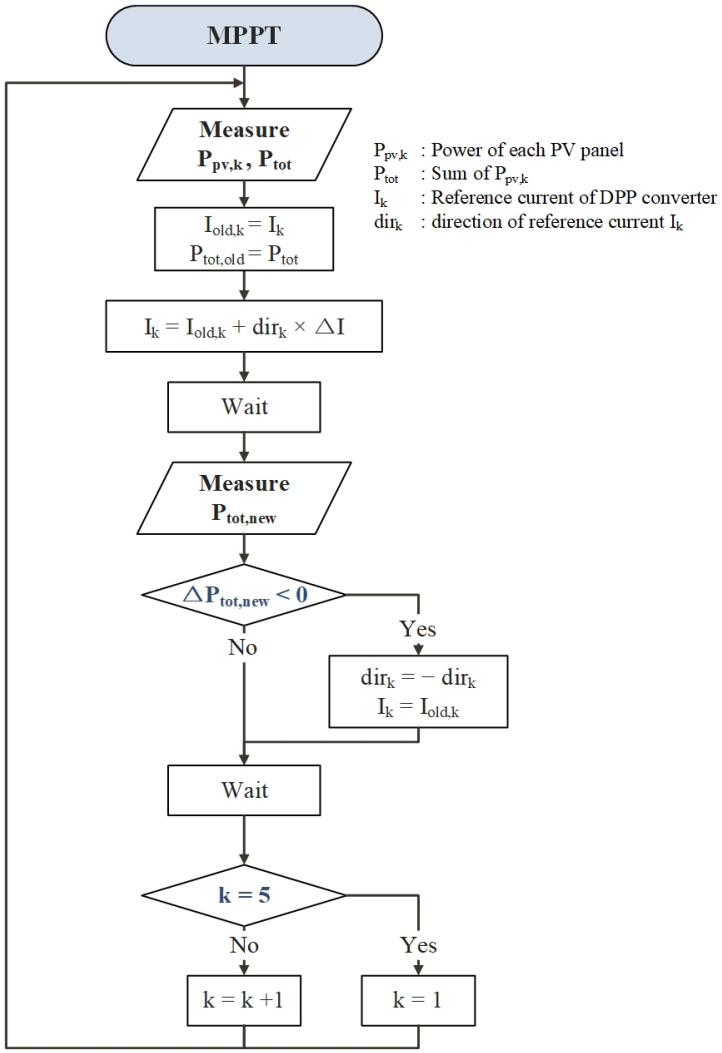


Figure 3.2: MPPT algorithm for the segmented DPP module

The number of required sensors for the control algorithm is also an important design aspect. As shown in Figure 3.3a, when the MPPT algorithm compares the present and previous total PV power, both voltage and current sensors are needed for each PV panel. Also, a current sensor is needed to control the DPP converter. This means that $3n$ sensors are needed for one module when $n$ is the number of PVs in one module. As the number of sensors used in the system increases, the calculation time of the controller becomes longer and the power loss through the sensors becomes larger.

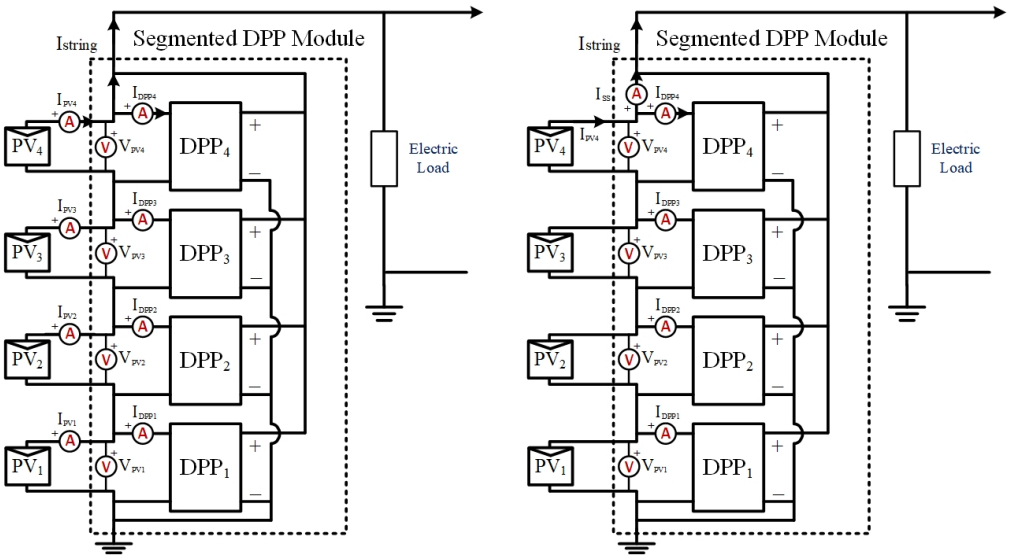


(a) $3n$ sensors (b) $2n+1$ sensors

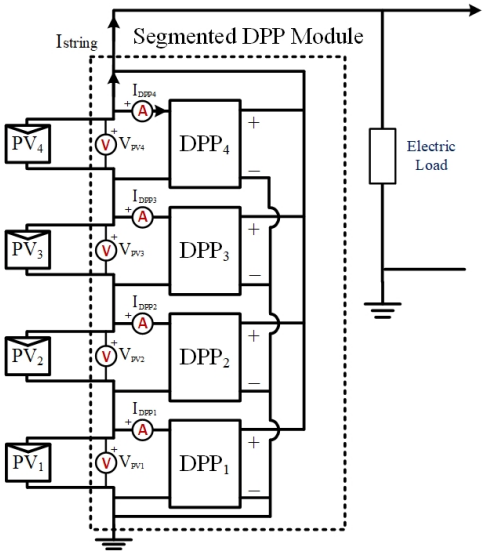


(c) $2n$ sensors

Figure 3.3: Sensor connection with (a,b) total power comparison, and (c) total voltage comparison

Instead of measuring the PV current directly, the primary-side current of converter $I_{DPP,k}$ and the substring current $I_{ss}$ can be used to decrease the number of sensors in one module as shown in Figure 3.3b. The current of the PV panel can be calculated with the sum of the primary-side current and

substring current ($I_{PV,k}$=$I_{DPP,k}$+$I_{ss}$). This method requires $2n+1$ sensors, which consists of PV voltage sensors, a current sensor for each DPP converter and a substring current sensor. However, with this method, there is a ripple in the sensed PV current, which is caused by the primary-side current ripple of the DPP converter. It causes the large power ripple in the sensed value, so it cannot measure the PV power correctly. To reduce this power ripple, an averaging function can be used, but it takes calculation time and makes the control mode complex. Another way to control this MPPT algorithm is using the relationships between voltage and power. The string current can be assumed as a constant according to the MPPT speed by the inverter control. Therefore, when the sum of $n$ PV voltages becomes maximum, the sum of the PV power also goes to the maximum point. As a second method to reduce the number of the sensors, the voltage-comparing MPPT algorithm can be used, as shown in Figure 3.4. This method requires $2n$ sensors, which are PV voltage sensors and a current sensor for each DPP converter. This algorithm has the minimum number of sensors, which can reduce the power losses and costs of the converter.

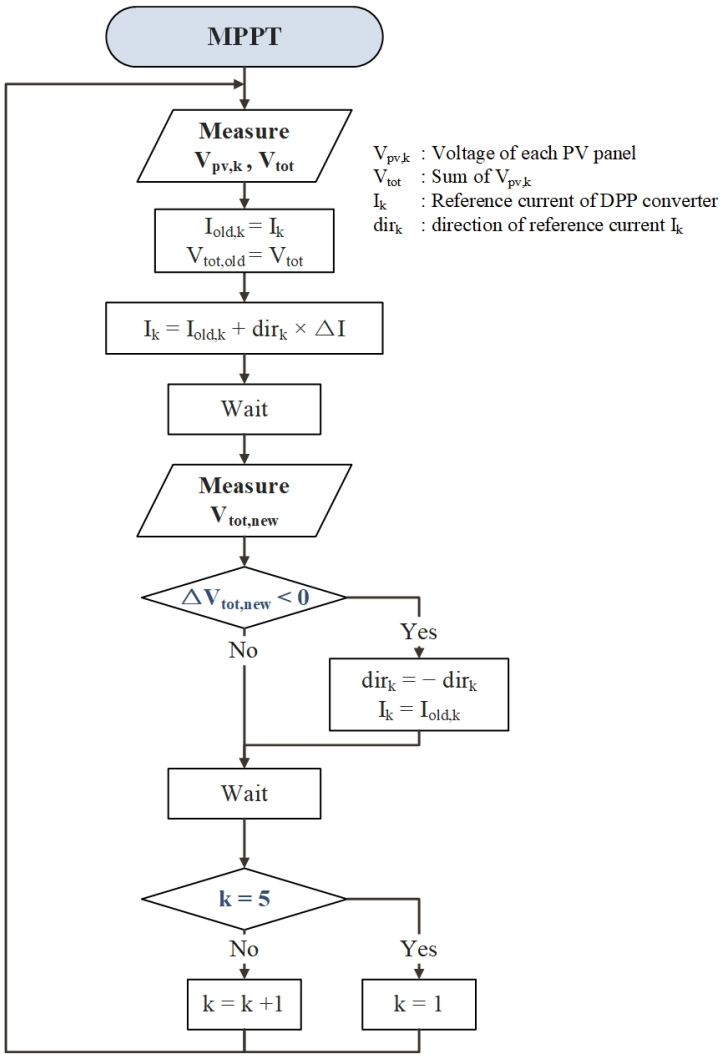


Figure 3.4: MPPT algorithm that minimize the number of sensor

## 3.2 Simulation Setup and Results

### 3.2.1 System and Algorithm Setup

To verify the algorithm and structure of the segmented DPP system, Matlab/Simulink was used. Figure 3.5 shows the simulation circuit of the segmented DPP system, which consists of four DPP converters and one unit converter. The bidirectional flyback converter was used for the DPP converter and the primary-side current ($I_{DPP}$) is controlled by a PI controller bidirectionally, as shown in Figure 3.6. Also, the primary-side voltage ($V_{pv}$) is measured and used as the input parameter of the segmented DPP system algorithm. After setting the algorithm as a reference current $I_{ref}$, the PI controller controls the converter to regulate $I_{DPP}$ to $I_{ref}$. In addition, the bidirectional boost (buck) converter was constructed as a unit converter as shown in Figure 3.7. The low voltage side is controlled by a PI controller to maintain the bus voltage at a constant value ($V_{ref}$). When controlling the low-side voltage, a hysteresis block was used to prevent the frequent changing between buck and boost modes, which would make the converter operation unstable. The high-voltage side of the unit converter is connected to the overall voltage of the four PVs.

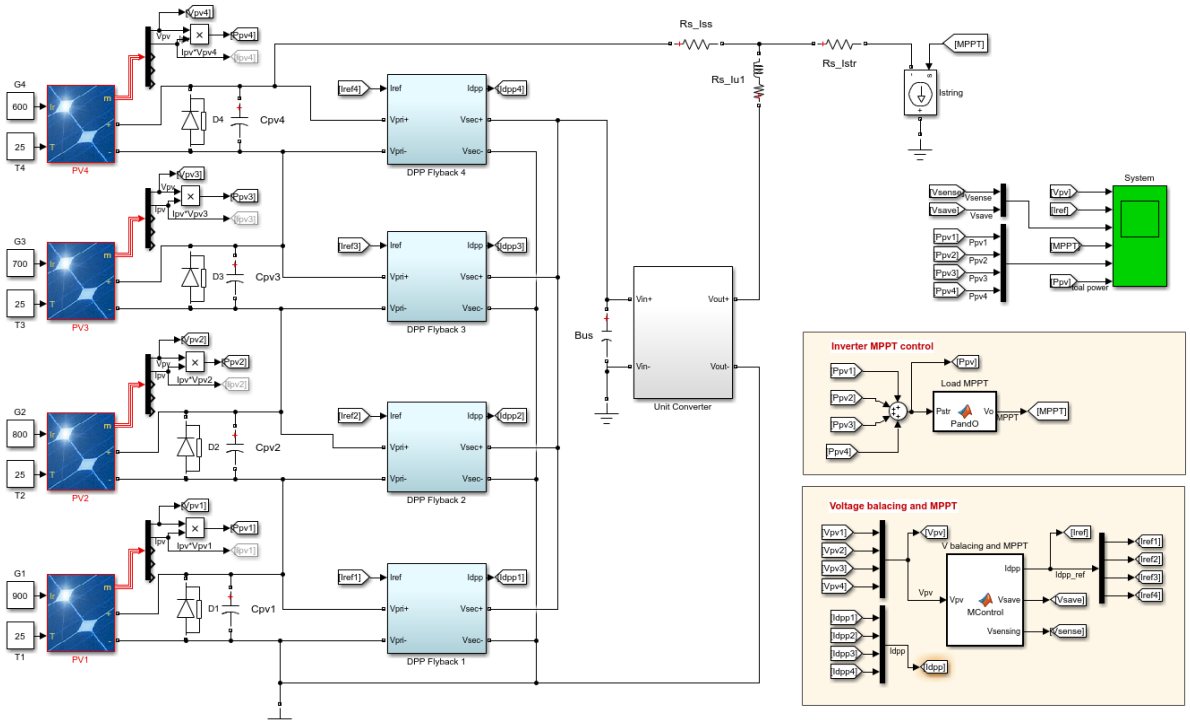


Figure 3.5: Simulation circuit of the segmented DPP system

For this simulation algorithm, a control block was implemented, which includes the voltage balancing and MPPT algorithm. As described in Section 3.1, when the PV voltages are out of a set boundary, the PVs do not operate near maximum power. At that time, the voltage balancing algorithm gathers the PV voltages within a certain range to recover quickly. In the case of MPPT algorithm, the sum of the PV voltages is compared with the previous sum value, and the converter sequentially tracks the maximum

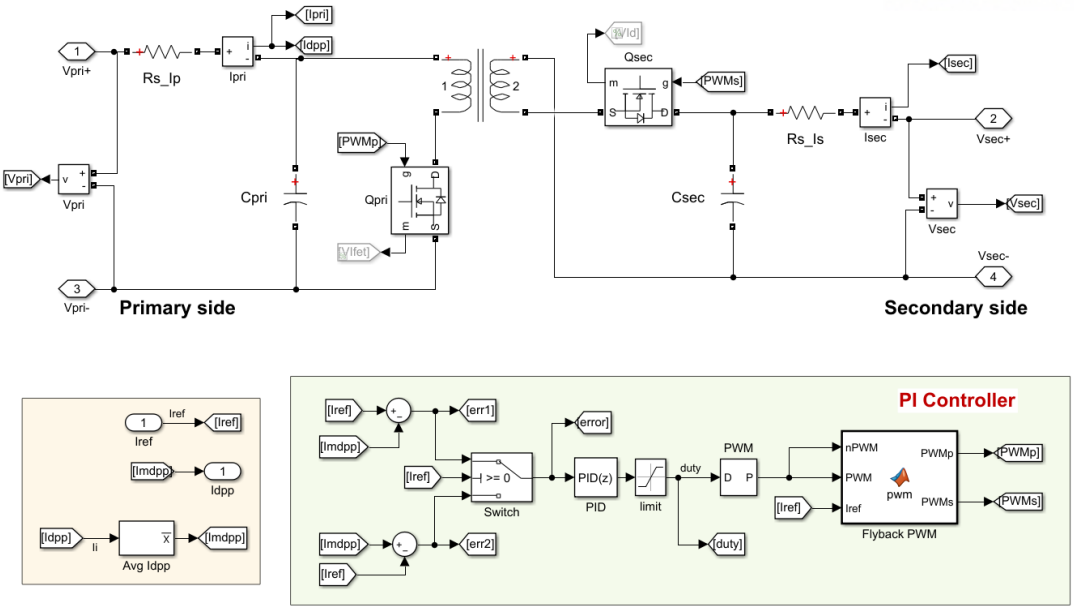


Figure 3.6: Simulation circuit of the bidirectional flyback converter

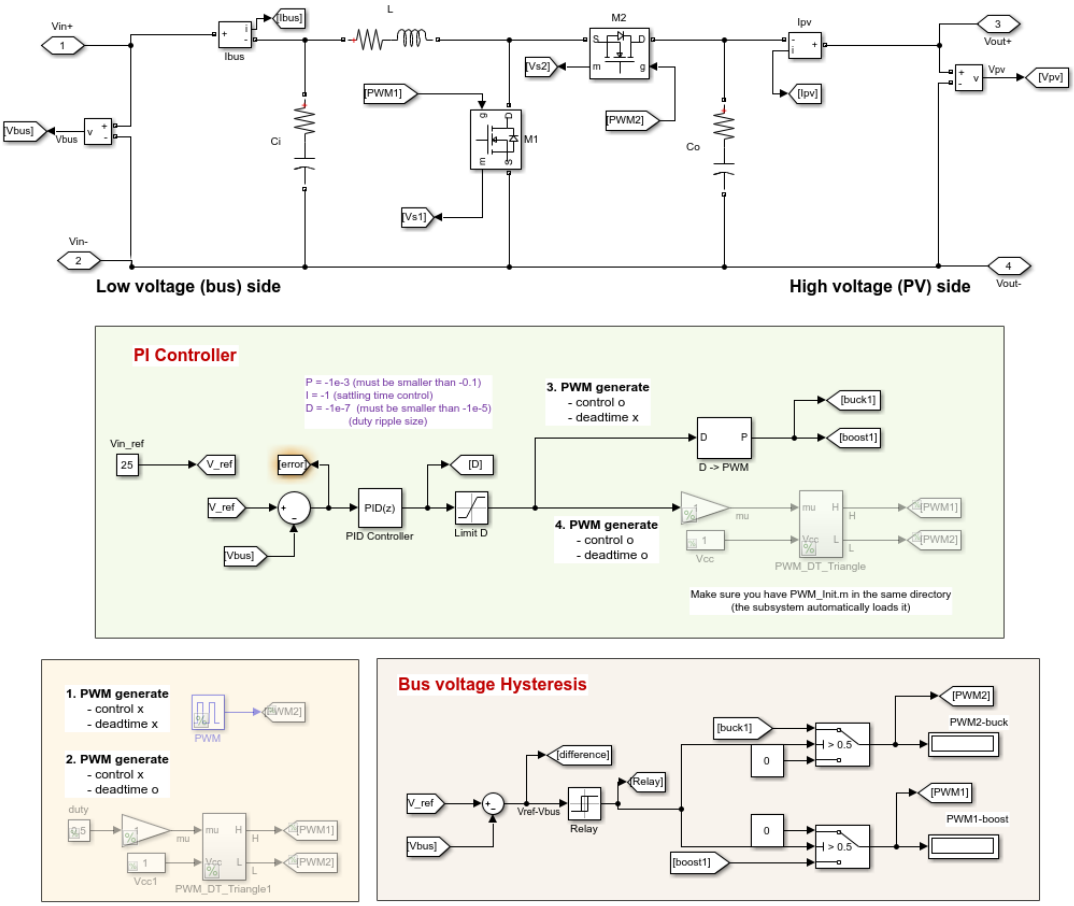


Figure 3.7: Simulation circuit of the bidirectional boost converter

power point of each PV. As shown in Figure 3.8, after the changing the reference current value, if the sum of the total voltage increases, the reference current will maintain the changed current value. In contrast, if the sum of the total voltage decreases, the reference current value goes back to the previous value. In this way, the four converters follow the algorithm in order.

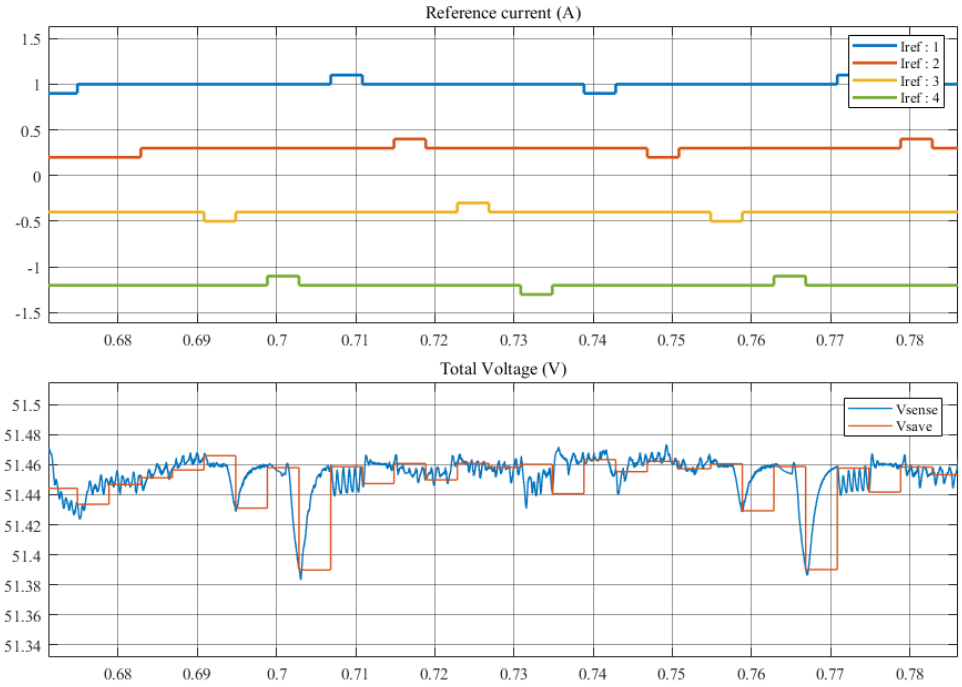


Figure 3.8: Operating MPPT algorithm showing reference current and total voltage

### 3.2.2 Simulation Results with One Module

The PV panel used in simulation has 106 W maximum power at 1000 W/m$^2$. The simulation was conducted for four PV panels, all at different irradiance values. The conditions of the four PVs are shown in Figure 3.9, which shows the open circuit voltage ($V_{oc}$), short circuit current ($I_{sc}$) and maximum power of each PV panel.

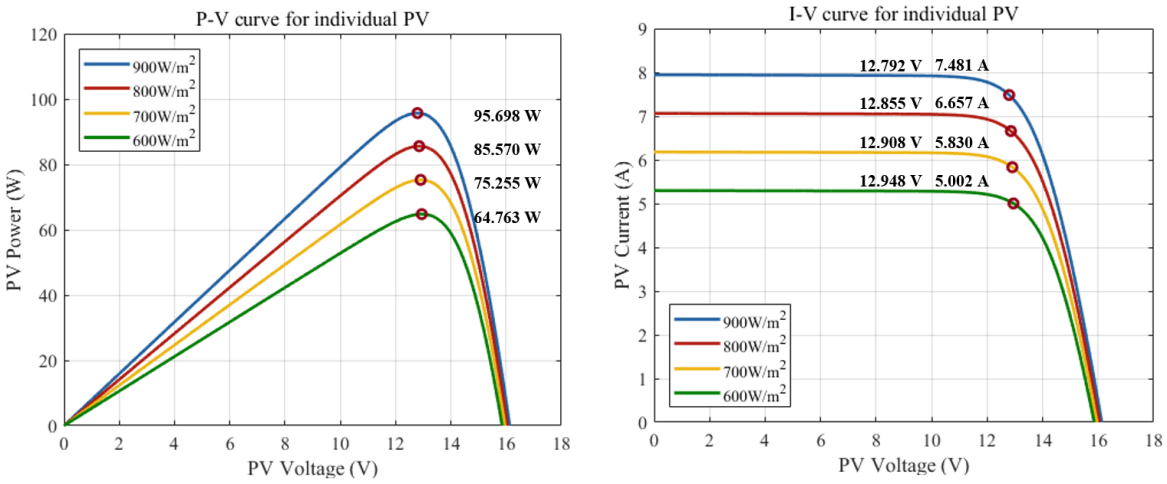


Figure 3.9: P-V and I-V curve of each PV panel used in the simulation

The segmented DPP system model was simulated with the inverter MPPT control block, which controls the string current using the P&O algorithm [26]. Figure 3.10 shows the system simulation results. Under this condition, PV1 and PV2 are in relatively strong sunlight and PV3 and PV4 are in weak sunlight. In this situation, as shown in Figure 3.10a, the reference current of the converters connected to PV1 and PV2 flow in the forward direction. Conversely, the reference currents connected to PV3 and PV4 flow in the reverse direction. Total output power is shown in Figure 3.10d, as the ideal maximum of the total PV power is 321 W, the DPP system properly followed the maximum power point.

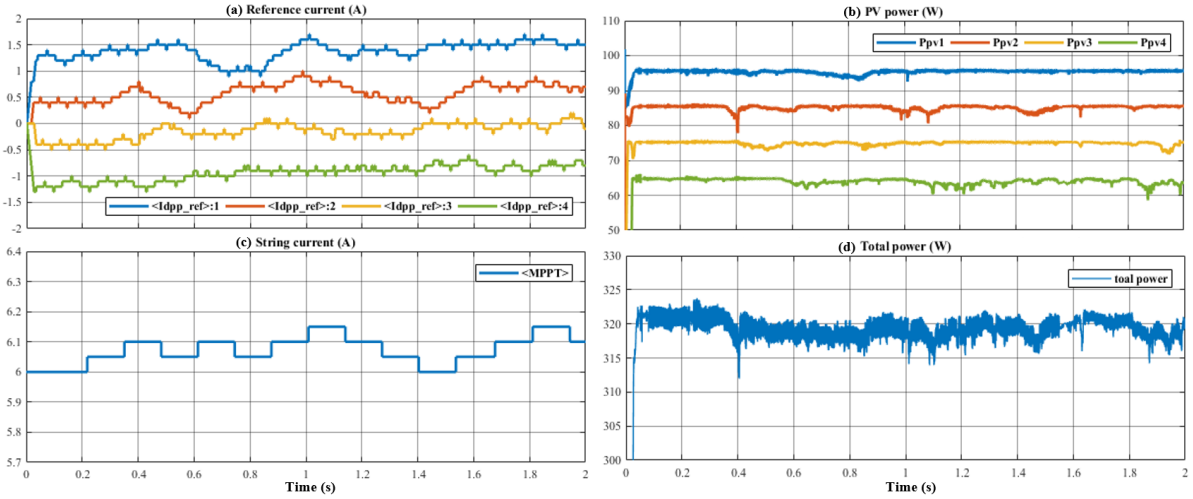


Figure 3.10: Simulation results of the segmented DPP system with unit converter

As mentioned in Section II, the segmented DPP system can consist of only flyback converters with-

out the unit converter. Figure 3.11 shows the simulation setup of the segmented DPP system without a unit converter. Due to the absence of this unit converter, the secondary side of the flyback converter is connected to the output of the four PV panels in this structure. The voltage balancing and MPPT algorithm are used as control blocks in simulation. As shown in Figure 3.12, this segmented DPP system also can control the panels at MPP, where the system output power maintains the total power as 320 W.

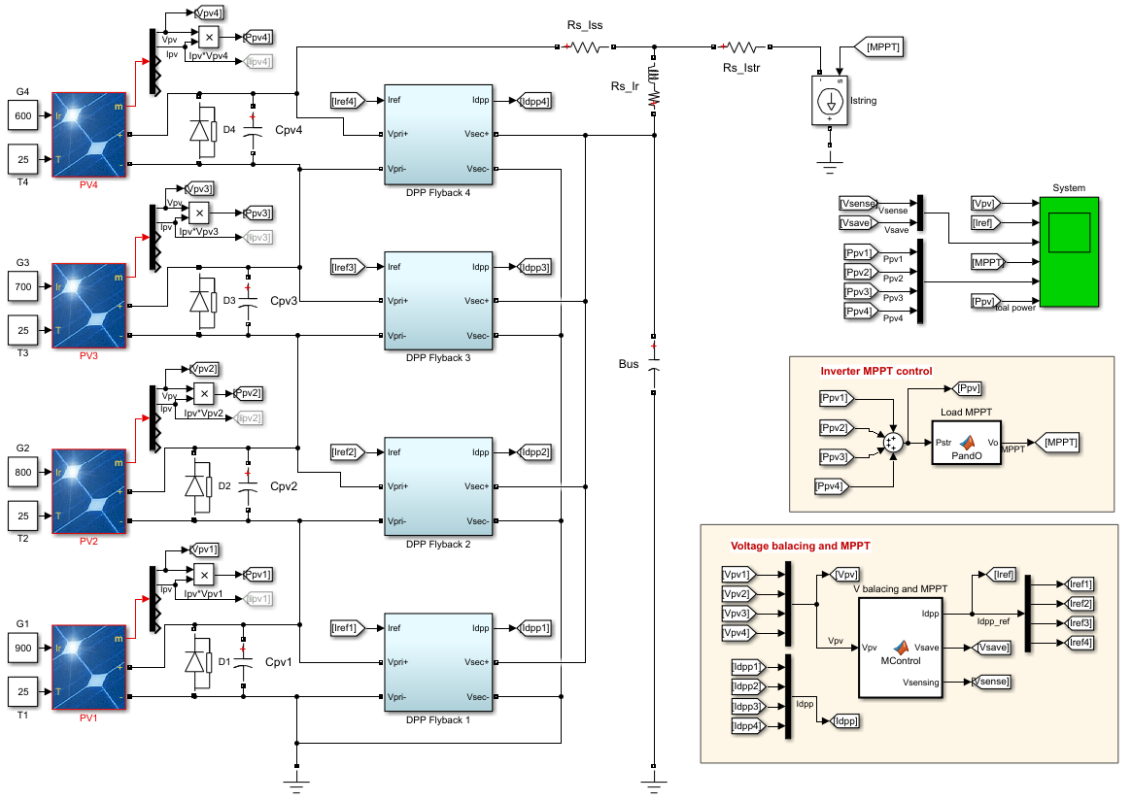


Figure 3.11: Simulation circuit of the segmented DPP system without unit converter

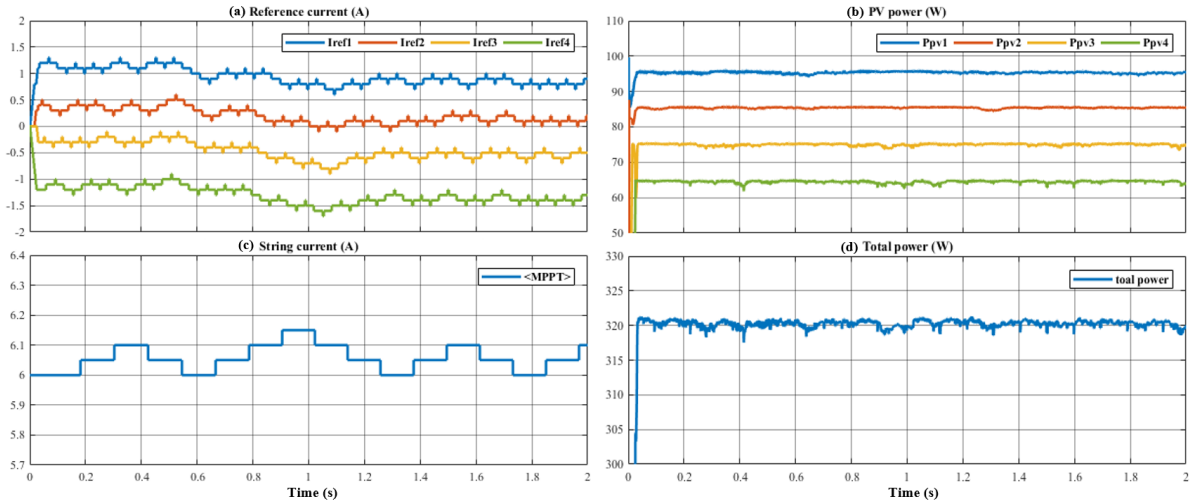


Figure 3.12: Simulation results of the segmented DPP system without unit converter

Then, the simulation was conducted with a current sweep to compare the output power curve of the

segmented DPP system with the series-connected system. The results are depicted in Figure 3.13, where the series-connected system has multiple peaks, which complicates the MPPT control in the inverter stage. Also, the maximum power is lower than the segmented DPP system.

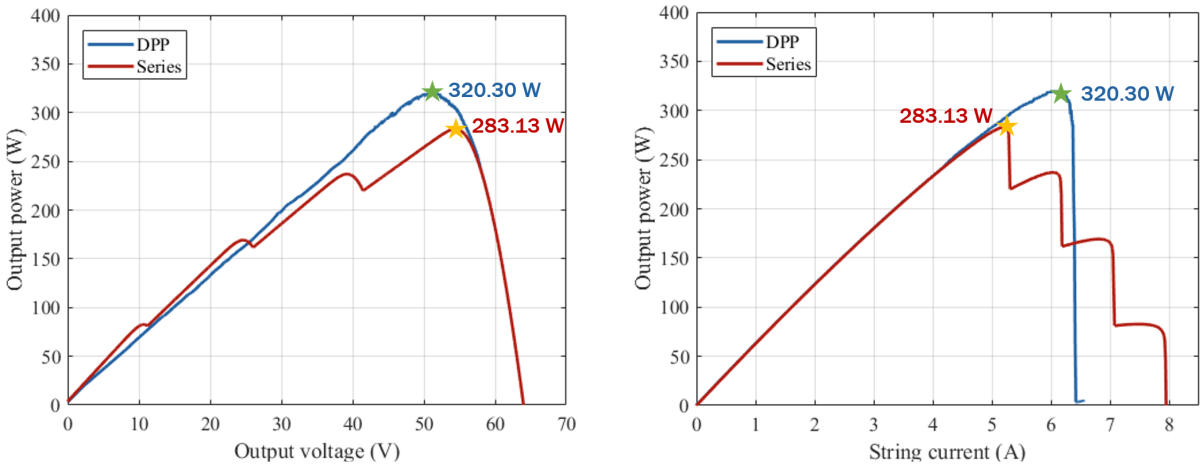


Figure 3.13: (a) P-V and (b) P-I curve comparing series and the DPP system in simulation

### 3.2.3 Simulation Results with Two Modules

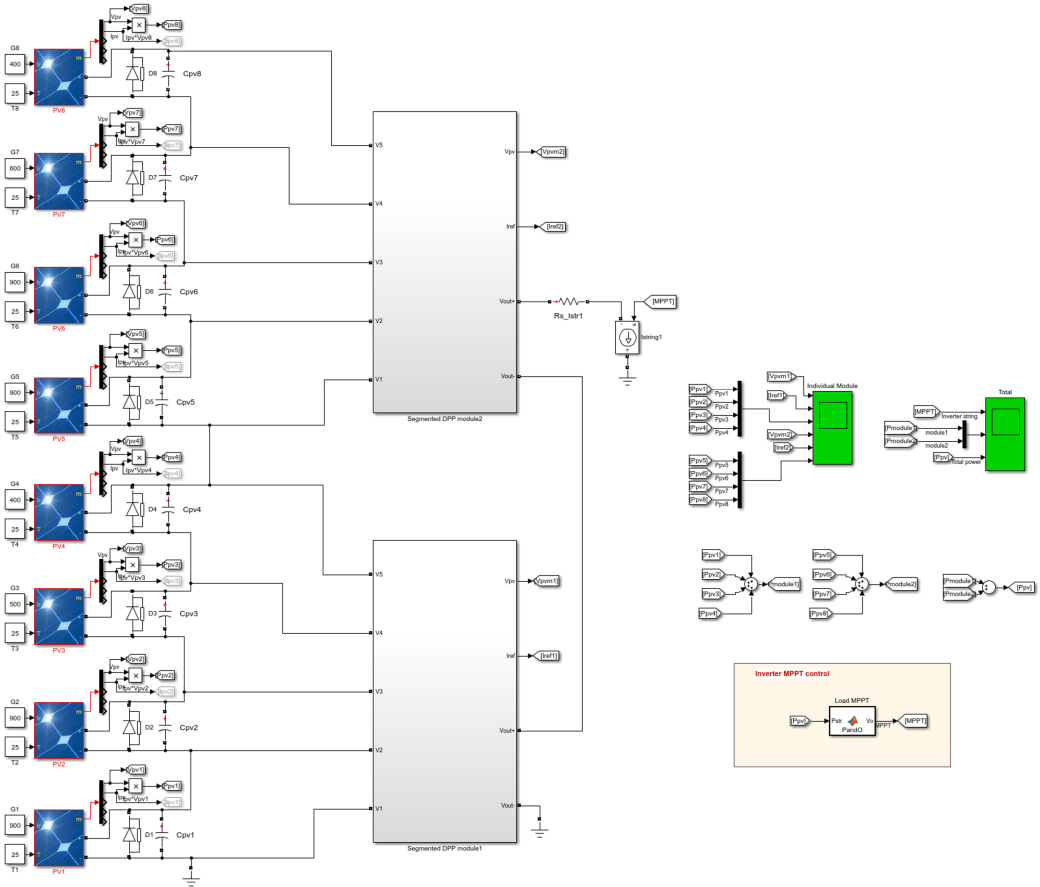

Figure 3.14: Simulation circuit of the segmented DPP system with two modules

The segmented DPP system is specially designed for the large-scale systems, which require multiple

segmented DPP modules. To confirm proper operation with multiple modules, the operation of two segmented DPP modules were simulated with eight PVs, as shown in Figure 3.14. The shading conditions of the PV panels are shown in Figure 3.15. The maximum power of PVs connected to module 1 is 95.7 W, 95.7 W, 54.1 W and 43.3 W, respectively, and the maximum power of PVs connected to module 2 is 95.7 W, 95.7 W, 64.76 W and 43.3 W, respectively. Figure 3.16a shows the current sweep results of the series connection and the segmented DPP system. As shown in the graph, the series-connected system has four peaks, which means the PVs cannot operate at their MPPs. With the segmented DPP modules, the PVs of module 1 produce 298.67 W and those of module 2 produce 287.21 W, which is shown in Figure 3.16b. Effectively, the PVs connected to one segmented DPP module act as a large panel. Therefore, when there are more than two segmented DPP modules, it looks like a large PV is connected in series to another large PV. They cannot compensate all eight PVs, but they can compensate small power differences between module 1 and module 2 with the module-level MPPT algorithm.

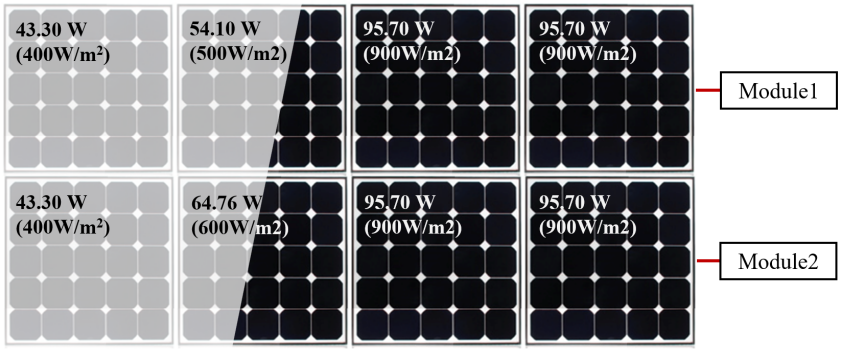


Figure 3.15: Simulated shading conditions for the PV panels

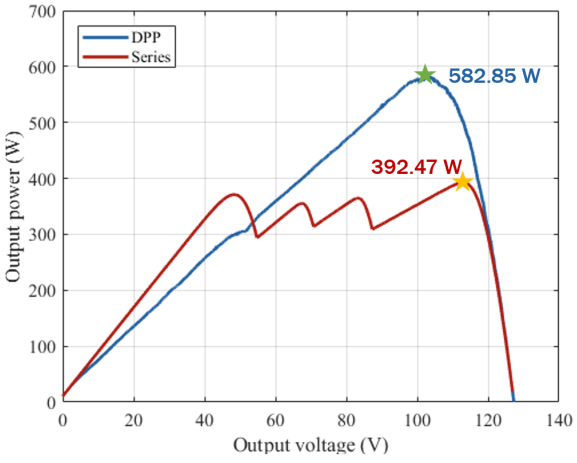


(a) P-V curve for the system output

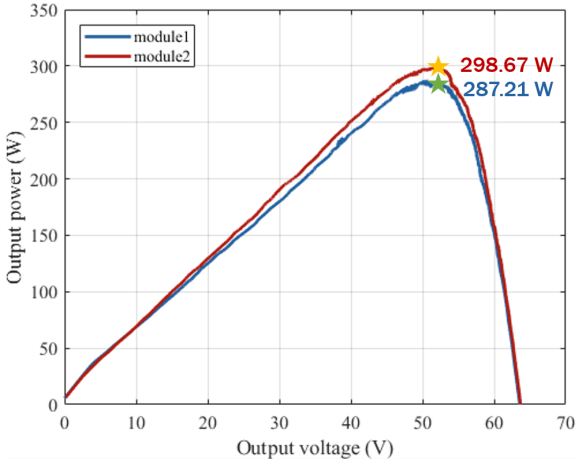


(b) P-V curve for the each moudule output

Figure 3.16: P-V curve for the two-module system simulation results

The segmented DPP system with two modules also simulated with an inverter P&O block. As shown in Figure 3.17, the output power of the segmented DPP system maintains MPP as 582 W. This shows the segmented DPP modules are able to interact with the inverter MPPT algorithm and optimize power produced bu the PVs of each module.

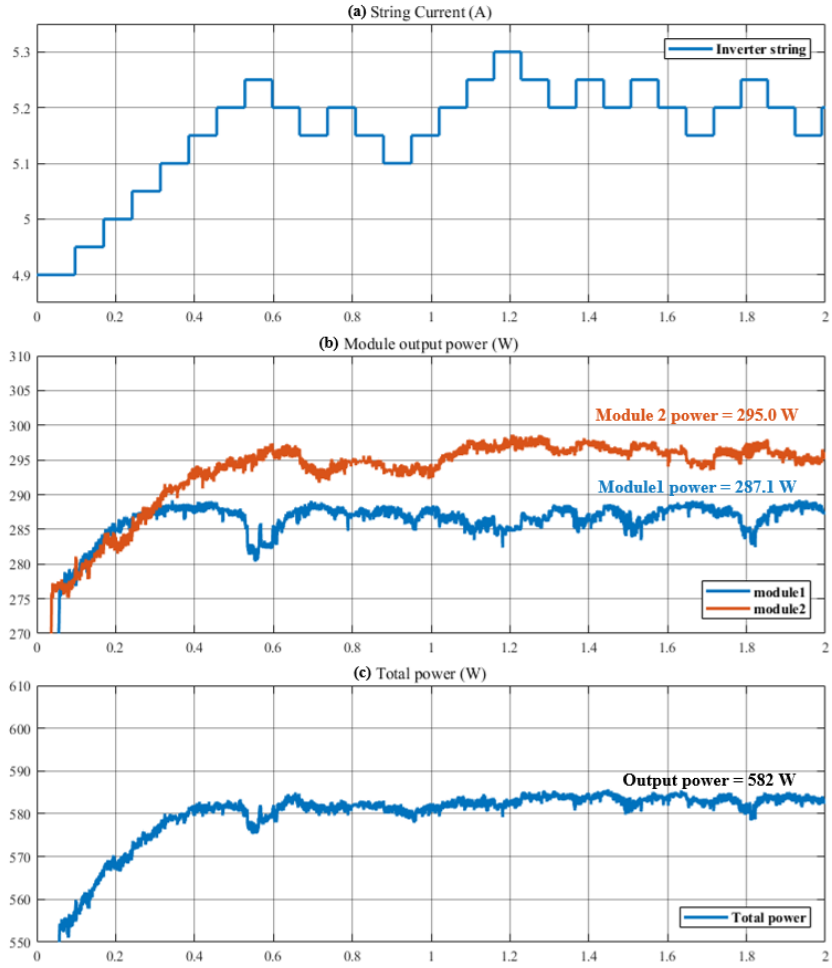


Figure 3.17: Simulation results of the segmented DPP system with two modules

# IV Prototype of the Segmented DPP System

In Section III, the algorithm and structure of the segmented DPP converter were verified through simulation. To test this system with real PV panels, the segmented DPP prototype converter was developed. As mentioned in Section II, there are two types of segmented DPP converters. Between the two systems, the system without unit converter was fabricated and tested. In this section, the design of the bidirectional flyback converter will be described.

## 4.1 DPP Converter

In the segmented DPP structure, the DPP converter controls each PV panel at its MPP and operates bidirectionally to transfer power from the PV panel to the string or vice versa. Also, the DPP converters need isolation between input and output because the DPP converter inputs are connected in series while the DPP converter outputs are connected in parallel, such that primary and secondary ground should be isolated. To satisfy these conditions, bidirectional flyback converters were selected for the topology of the DPP converters, which have been shown in [27, 28].

### 4.1.1 Bidirectional Flyback Converter Topology

In the bidirectional flyback converter, the diode of the unidirectional flyback converter is replaced by a MOSFET switch for bidirectional operation. The internal body diode of this MOSFET acts as a diode while transferring the power bidirectionally. The flyback converter has two operation modes, one is continuous conduction mode (CCM) and the other one is discontinuous conduction mode (DCM). In the case of CCM, the input side switch turns on when the output side current flows through the body diode. In this mode, the body diode needs more time to complete reverse recovery due to the characteristics of the MOSFET body diode. This causes a large peak and ripple current through the input-side switch, which causes reverse recovery loss, as shown in Figure 4.1a. However, in DCM, the input side switch is turned on when the output side current has already reached zero, which means there is no reverse recovery loss [29, 30]. Also, there is no right half plane zero in the DCM operation, which can make the compensation feedback loop easier in control. Therefore, the bidirectional flyback converter for the DPP converter was designed for the DCM.

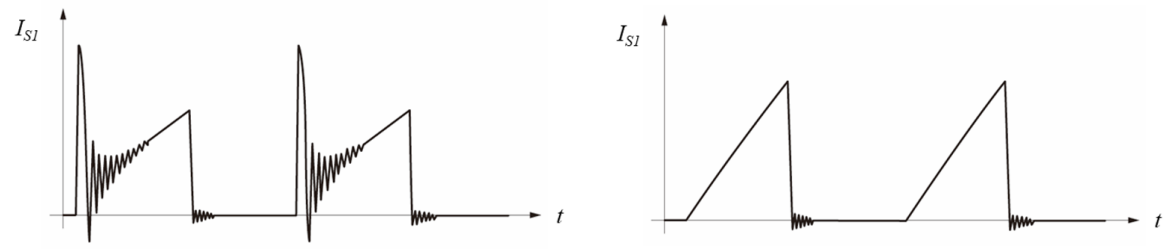


(a) Switch current in CCM

(b) Switch current in DCM

Figure 4.1: Input side switch current of the bidirectional flyback converter [30]

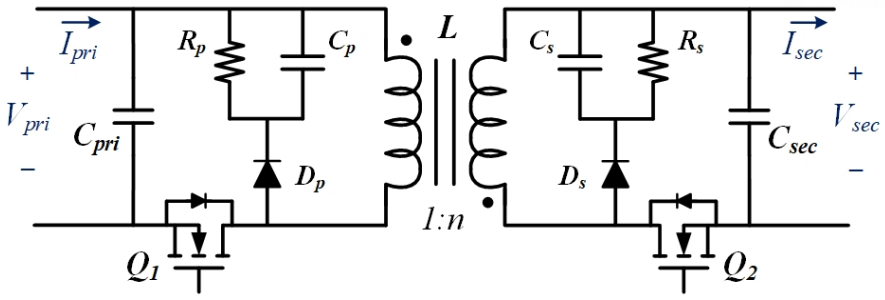


Figure 4.2: Circuit of the bidirectional flyback converter

The input and output voltage relation in the flyback converter for the DCM can be presented as

$$\begin{aligned} \frac{V_{in}^2 D^2 T}{2L_m} &= \frac{V_{out}^2}{R} = V_{out} I_{out} \\ \frac{V_{out}}{V_{in}} &= D\sqrt{\frac{RT}{2L_m}} = D\sqrt{\frac{V_{out} T}{2L_m I_{out}}} \end{aligned} \tag{1}$$

where $V_{in}$ is input voltage, $V_{out}$ is the output voltage, $D$ is duty and $R$ is load resistance of the flyback converter. $T$ is the switching period and $L_m$ is the coupled inductor magnetizing inductance [31]. The flyback converter for the DPP converter operates in two directions. First, in the forward direction, the input voltage and current becomes $V_{pri}$ and $I_{pri}$ and the output voltage and current is $V_{sec}$ and $I_{sec}$, so from equation (1), the voltage and duty in forward direction $D_1$ can be derived as

$$\frac{V_{sec}}{V_{pri}} = D_1\sqrt{\frac{V_{sec} T}{2L_{mp} I_{sec}}} \tag{2}$$

Solving for $D_1$,

$$D_1 = \sqrt{\frac{2L_{mp} V_{sec} I_{sec}}{V_{pri}^2 T}} = \sqrt{\frac{2L_{mp} I_{pri}}{V_{pri} T}} \tag{3}$$

where $L_{mp}$ is the primary-side and $L_{ms}$ is secondary-side magnetizing inductance of the coupled inductor. In the same way, the reverse direction operation has the input voltage and current as $V_{sec}$ and $I_{sec}$ and the output voltage and current as $V_{pri}$ and $I_{pri}$. Also, by using the notation of Figure 4.2, the output current is $-I_{pri}$. Therefore, the voltage and the duty in the reverse direction $D_2$ can be derived as

$$\frac{V_{pri}}{V_{sec}} = D_2\sqrt{\frac{V_{pri} T}{2L_{ms}(-I_{pri})}} \tag{4}$$

Solving for $D_2$,

$$D_2 = \sqrt{\frac{2L_{ms} V_{pri}(-I_{pri})}{V_{sec}^2 T}} \tag{5}$$

Equations (3) and (5) show that both duty $D_1$ and $D_2$ can be presented with $I_{pri}$ and they are proportional to the square root of $I_{pri}$, which is the parameter of the reference control value in the algorithm. Therefore, the primary-side current $I_{pri}$ of the flyback converter is controlled by changing the duty of the flyback converter. Also, according to the sign of $I_{pri}$, the power flow of the converter can be distinguished. When the $I_{pri}$ is positive, power flows in the forward direction and when the $I_{pri}$ is negative, power flows in the reverse direction through the flyback converter.

### 4.1.2 Bidirectional Flyback Converter Design

The open-circuit voltage, $V_{oc}$ and the number of the PV in one segmented DPP module, $n$, determines the voltage rating of the flyback converters. The primary side should be rated at $V_{oc}$ and the secondary side should be rated at $n$ times $V_{oc}$. Also, the nominal input voltage of the DPP converter is the voltage at MPP, $V_{mpp}$, because the converter will usually operate at $V_{mpp}$. For this work, $V_{oc} = 16$ V, $V_{mpp} = 12.8$ V and $n = 4$. The converter current rating is directly related to the amount of expected current mismatch of the PV panels. Work in [32] identified power ratings of 15-17% to compensate PV cell degradation in PV-to-bus converter systems. For this work, the current limit was chosen at 2.0 A for PV panels with MPP current of 8.3 A, which is equivalent to 24% rating.

For designing the entire flyback converter system, considering the ground of the primary and secondary side is important, which must be isolated. To operate the two MOSFET switches, the gate drivers for each MOSFET are needed. Both the primary and secondary-side gate drivers need 12 V voltage supply through an LDO. If this voltage supply is from the primary-side, the voltage input to the LDO can be unstable, because the PV voltage can be lower than 12 V depending on the conditions of the PVs. For this reason, it is necessary to supply the LDO from the secondary-side voltage, which is the sum of $n$ PV voltage and can supply a more reliable voltage. However, for the primary-side gate driver, the ground should be separated from the secondary ground. Therefore, a small isolated DC-DC converter was used for the primary-side gate driver and the LDO was used for the secondary-side gate driver. Figure 4.3 shows the diagram of the bidirectional flyback converter. As shown, each flyback converter needs one DC-DC converter and two LDOs for supplying power to the gate driver and sensors.

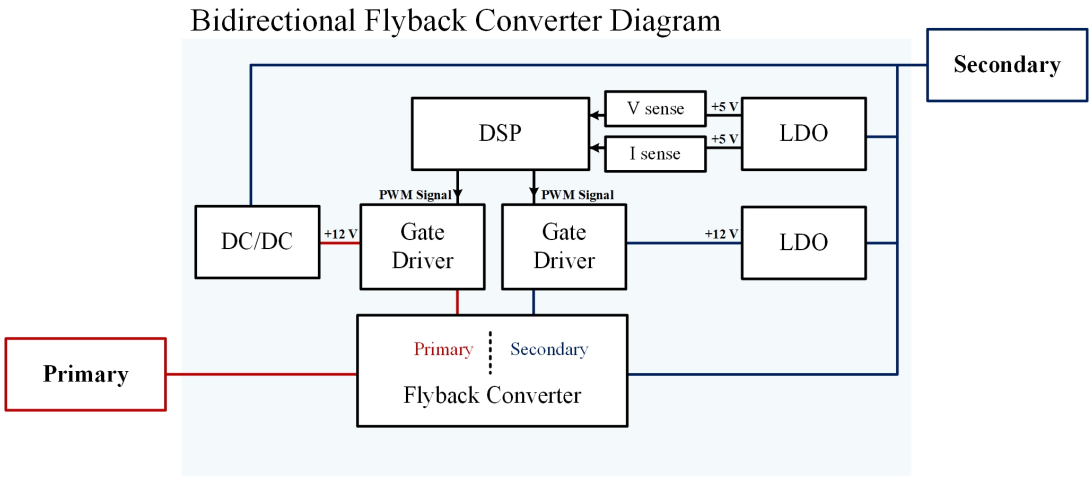


Figure 4.3: Diagram of the bidirectional flyback converter

The PCB layout design of the bidirectional flyback converter is shown in Figure 4.4. The red routing represents the top side and blue routing represents the bottom side of the PCB. The fabricated bidirectional converter is shown in Figure 4.5, which size 130 mm by 63 mm in area. The design parameters of this converter are shown in Table 4.1. The magnetizing inductance is 6.5 µH and the turns ratio of the coupled inductor is 4, which is designed for DCM operation. Figure 4.6 shows the measured efficiency of the designed flyback converter, which has 89.04% in the forward direction and 86.15% efficiency in

the reverse direction at 25 W of power, which is full load. This is the power stage efficiency, which does not include LDO and sensor losses. With the LDO and sensor losses, the flyback converter has 87.75% efficiency in the forward direction and 83.81% efficiency in the reverse direction at the full load.

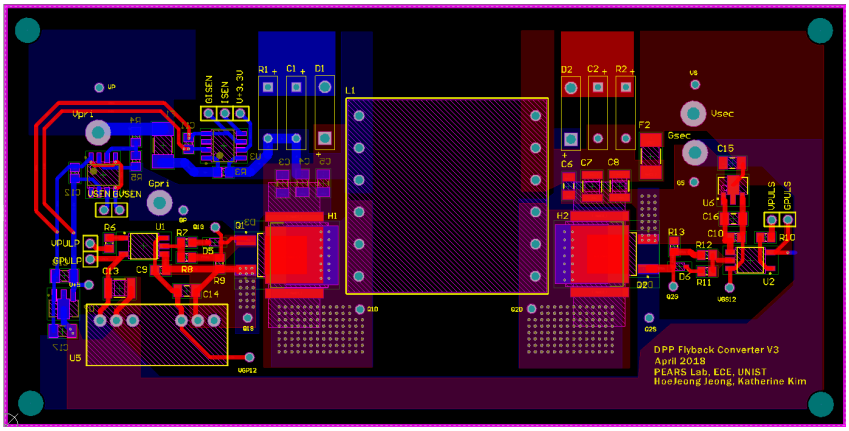


Figure 4.4: PCB layout of the bidirectional flyback converter

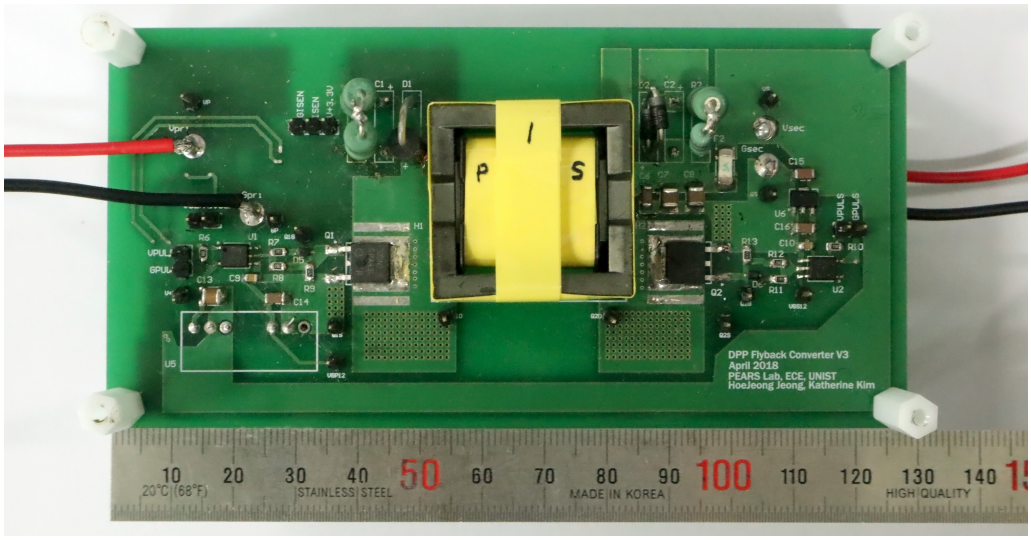


Figure 4.5: Fabricated bidirectional flyback converter

| | | Primary | Secondary |
|---|---|---|---|
| **Power** | **Voltage (V)** | 12.8 | 51.2 |
| | **Current (A)** | 2.0 | 0.5 |
| | **Switching frequency (kHz)** | 100 | |
| **Coupled inductor** | **Turn number** | 6 | 24 |
| | **Magnetizing inductance (μH)** | 6.5 | 101.2 |
| | **Leakage inductance (μH)** | 0.213 | 3.031 |
| **Snubber** | **Capacitance (nF)** | 300 | 10 |
| | **Resistance (Ω)** | 470 | 2500 |

Table 4.1: Design parameters of the bidirectional flyback converter

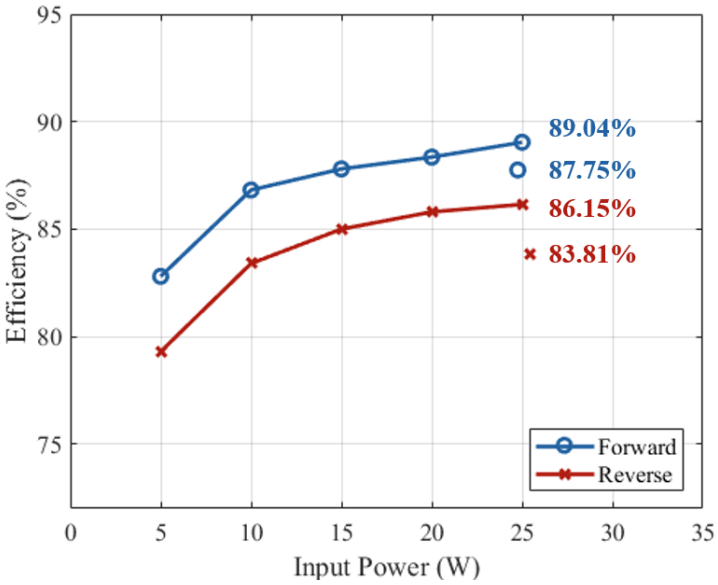


Figure 4.6: Efficiency of the bidirectional flyback converter

## 4.2 System Implementation

The segmented DPP module is composed of four DPP converters, which are the designed bidirectional flyback converters mentioned in the previous section. The converters are connected to the terminal blocks with wires and four converters are controlled by a TMS320F28335 DSP. Figure 4.7 shows the flyback converters and controller, which were used in one segmented DPP module.

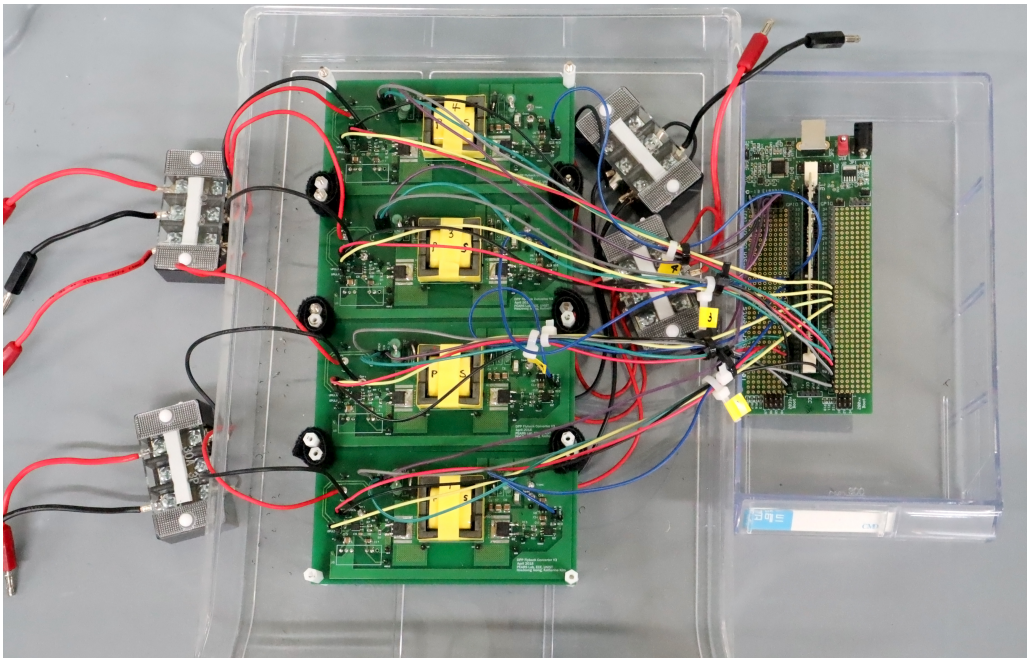

Figure 4.7: Implemented segmented DPP module

# V System Performance Evaluation

To verify this segmented DPP system, the developed prototype module was tested in experiment. The prototype was composed of four bidirectional flyback converters, and the control algorithm was implemented with the TMS320F28335 DSP controller. The PV panels consists of 25 Silicon PV cells and they are connected in series. The PV panels have maximum power at 8.3 A and 12.8 V, which generate 105 W under 1000 W/m$^2$ and 25°C. To measure the experimental results, a power analyzer and electric load were used. The power analyzer measures the power of the PV panels and the electric load is used for measuring the load power. These two types of equipment are connected to a computer with GPIB and USB communication interface to send data to a computer. Figure 5.1 shows the diagram of the experimental setup and equipment. The indoor and outdoor experiments were conducted with this equipment setup, and the series-connected system and the segmented DPP system are compared under various light conditions.

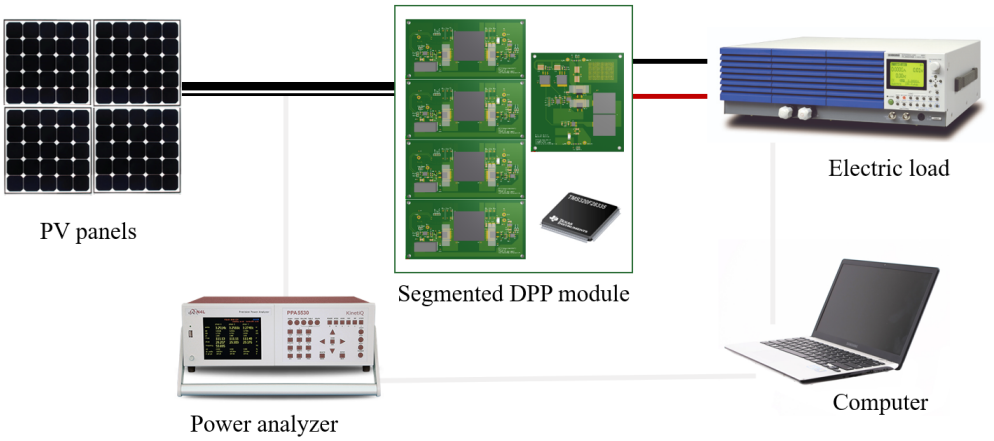


Figure 5.1: Experimental setup with equipment

Because the irradiance conditions and temperature of the PV panels are keep changing, the PV power are not perfectly the same for all experimental conditions. In this reason, comparing output power directly is not a fair comparison. Therefore, the following standards are used to compare the system. MPP tracking efficiency is defined as

$$\eta_{MPPT} = \frac{\sum_{k=1}^{n} P_{PV,k}}{\sum_{k=1}^{n} P_{MPP,k}} \tag{6}$$

where $P_{PV,k}$ is the power produced by PV $k$ actually and $P_{MPP,k}$ is the true maximum power of PV $k$. In other words, the sum of $P_{PV,k}$ is the generated PV power from $k$ PV panels and the sum of $P_{MPP,k}$ means the ideal maximum power of the system. Next, module efficiency is defined as

$$\eta_{mod} = \frac{P_{out}}{\sum_{k=1}^{n} P_{PV,k}} \tag{7}$$

where $P_{out}$ is the output power at load MPP, and this module efficiency includes the converter loss. Lastly, system efficiency is defined as

$$\eta_{sys} = \frac{P_{out}}{\sum_{k=1}^{n} P_{MPP,k}} = \eta_{MPPT} \times \eta_{mod} \tag{8}$$

which is mainly used standard to evaluate the overall performance of the segmented DPP system.

## 5.1 Indoor Experiment

With the segmented DPP prototype, the experiment was conducted with with halogen lamps on each PV panels, as shown in Figure 5.2. First, the current sweep was conducted with series-connected system, and then the current sweep with the segmented DPP system was conducted under the same condition. To compare the system efficiency of the series-connected system and the segmented DPP system, the experiment was conducted under relatively even light and mismatched uneven light.

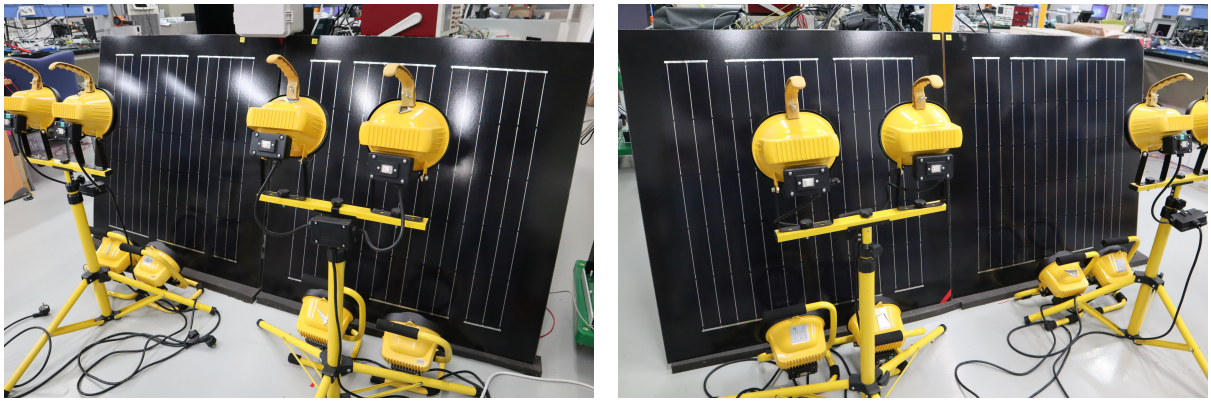

Figure 5.2: Indoor experiment setup with PVs and halogen lamps

### 5.1.1 Even Lighting Conditions

To test the system under even lighting conditions, the same number of the halogen were used. In Figure 5.3, the left graphs show the individual PV graphs that were acquired during the sweep, from which the true MPP of each PV is calculated. The right graphs show the input PV power, which is the sum of the PV power, and output power for the segmented DPP module. From this data, the MPP tracking, module, and system efficiency can be determined for the given lighting condition. Results for the series-connected case are shown in Figure 5.3a, where the ideal maximum power is 58.93 W, but MPP tracking efficiency is 90%, which results in a maximum input power of 53.05 W and output power of 52.05 W. The resulting system efficiency is 89.05%.

Results for the segmented DPP prototype are shown in Figure 5.3b, where MPP tracking efficiency increases to 95.35%, but with the additional converter losses the module efficiency decreased to 89.00% such that system efficiency is 84.86%. The system efficiency decrease is attributed to low PV input power. The narrow spectrum of the halogen lamps leads to the PV panels only producing about 18% of their rated power in the indoor experiment. Thus, converter losses in segmented DPP module have a bigger impact on the efficiency than at the nominal power level.

### 5.1.2 Uneven Lighting Conditions

Next, the prototype was tested under uneven lighting, where four halogen lamps were used on PV3, three on PV1 and PV2, and two on PV4. Experimental results are shown in Figure 5.4, where the left graphs show the power of each PV panel. Results for the series-connected string are shown in Figure 5.4a, where the string power curve shape changes and local MPP are visible. The MPP voltage of

| | Individual PV Panels | | | | | Maximum Power Point | | | | | System Performance | |
|---|---|---|---|---|---|---|---|---|---|---|---|---|
| System | $PV_1$ (W) | $PV_2$ (W) | $PV_3$ (W) | $PV_4$ (W) | $PV_{sum}$ (W) | $P_{in}$ (W) | $P_{out}$ (W) | $V_{out}$ (V) | $I_{out}$ (A) | Module efficiency | Tracking efficiency | System efficiency |
| **Indoor even condition** | | | | | | | | | | | | |
| **Series** | 13.91 W | 14.36 W | 17.06 W | 13.59 W | 58.93 W | 53.05 W | 52.49 W | 48.6 V | 1.08 A | 98.93% | 90.01% | **89.05%** |
| **Segmented DPP** | 13.29 W | 12.91 W | 17.99 W | 12.79 W | 56.98 W | 54.33 W | 48.35 W | 44.77 V | 1.08 A | 89.00% | 95.35% | **84.86%** |
| **Indoor uneven condition** | | | | | | | | | | | | |
| **Series** | 12.36 W | 12.83 W | 18.91 W | 5.77 W | 49.87 W | 36.85 W | 35.73 W | 37.61 V | 0.95 A | 97.00% | 73.88% | **71.64%** |
| **Segmented DPP** | 12.34 W | 13.28 W | 19.24 W | 6.44 W | 51.30 W | 49.02 W | 42.53 W | 46.74 V | 0.91 A | 86.77% | 95.55% | **82.91%** |

Table 5.1: Test results under indoor lighting conditions

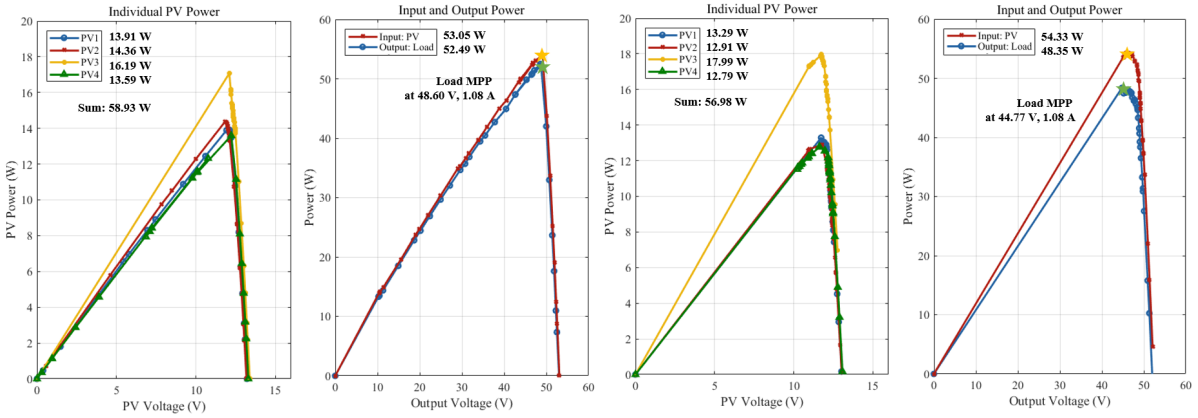


(a) Series-connected system (b) Segmented DPP system

Figure 5.3: P-V curve in even indoor lighting conditions

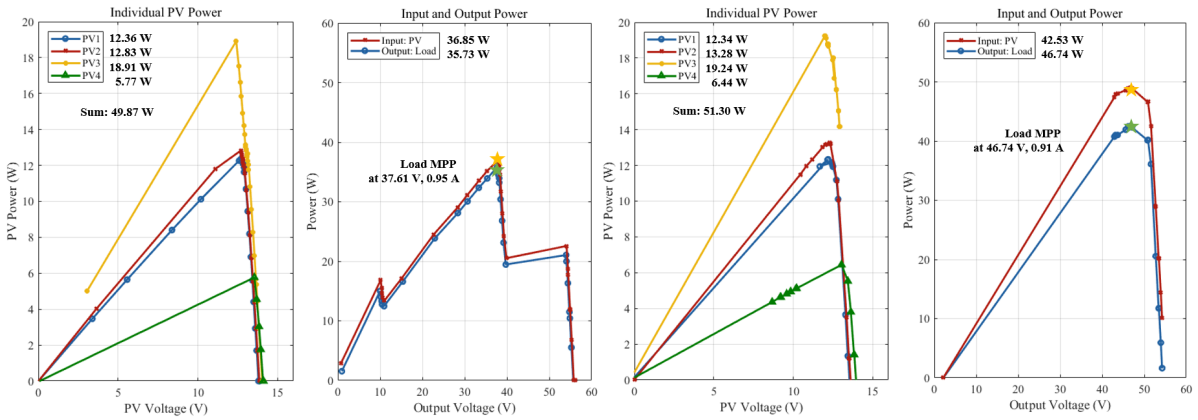


(a) Series-connected system (b) Segmented DPP system

Figure 5.4: P-V curve in uneven indoor lighting conditions

the string is 37.61 V, which means that only 3 PVs are active and the weakest panel (PV4) is bypassed. The resulting MPP tracking efficiency is 73.88%, module efficiency is 97.00% and system efficiency is 71.64%.

Figure 5.4b shows results using the segmented DPP converter is the uneven lighting conditions. The string power curve is smooth and convex such that there is only one clear MPP, which ensures that the inverter-level MPPT does not get caught operating at a non-global local MPP. Also, the voltage at MPP with the segmented DPP system is 49.74 V, which indicates that all four PV panels are generating power near their MPP. With the segmented DPP module, the MPP tracking efficiency is 95.55%, module efficiency is 86.77% and system efficiency is 82.91%. As shown in the results, under the uneven lighting condition, the system efficiency is increased by 11% compared to the series case. The results of the indoor lighting conditions are summarized in Table 5.1.

### 5.1.3 Discussion

This indoor testing with the halogen lamps has an advantage in its ability to control the number of the lights. However, as shown in Figure 5.3a, even in the even lighting case, the MPP of each PV panel is different. This is because small mismatch due to slight angle differences and light intensity reduction as each bulb ages. Also, the lamps cannot generate and spread the light in the same way as natural sunlight. Due to this limitation, they can generate only 13% of the PV's rated power. For these reasons, it is difficult to extensively test the prototype in various conditions with the indoor halogen lamp setup.

## 5.2 Outdoor Experiment

Due to the power limitation of the indoor testing, the system was experimented under natural sunlight. The testing setup is shown in Figure 5.5. Tests were conducted on a relatively clear day when the direct irradiance was approximately 1300 W/m$^2$ under even conditions and then partially shaded to create uneven shading as shown in Figure 5.6.

(a) Four PV panels and irradiance meter

(b) Equipment setup for the outdoor testing

Figure 5.5: Outdoor experimental setup with PVs and equipment

### 5.2.1 Even Lighting Conditions

First, the PV panels were unshaded and the results are shown in Figure 5.7. Results for the series-connected case are shown in Figure 5.7a, where the ideal maximum power is 266.9 W with near exact MPP tracking, which results in output power of 258.9 W. The resulting system efficiency is 96.97%. Results for the segmented DPP prototype are shown in Fig. 5.7b, where MPP tracking efficiency is 99.66% and module efficiency is 95.05%, such that system efficiency reaches 94.74%. Due to the higher PV power, the converter losses are less significant, resulting in improved system efficiency compared to the indoor case.

### 5.2.2 Unven Lighting Conditions

Then, in one panel a column of five PV cells was shaded by 50% using the paper sheet, as shown in Figure 5.6 and the test was run again under approximately 1300 W/m$^2$ irradiance. Results for the series-connected string are shown in Figure 5.8a, where the string power curve again shows local MPP. The resulting MPP tracking efficiency decreases to 84.71%, module efficiency is 97.53% and resulting system efficiency is 82.61%. Then, with the segmented DPP module, tracking efficiency increases to 96.72% and module efficiency is 94.72%, which results in a system efficiency of 91.38%. Compared to the series case, the segmented DPP system increased system efficiency by 8.77%.

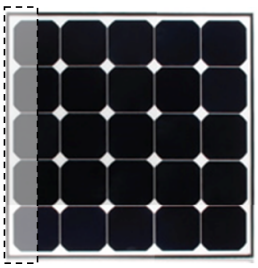

Paper transmittance: 27-30%

(a) Shaded panel

(b) PV panel setup with shaded PV panel

Figure 5.6: Shading condition in outdoor testing

### 5.2.3 Discussion

These results show that employing the segmented DPP module increases the system efficiency by over 8-10% in uneven lighting conditions. It also removes local MPPs from the power curve to enable better interaction with the inverter MPPT algorithm and consistently track the true MPP. In the outdoor tests, the segmented DPP module efficiency reached 95%, and there is still room for improvement through design optimization to reduce losses. Under this outdoor experiment, the PV panel receives natural sunlight that can generate power at realistic levels. However, the conditions of irradiance and PV temperature continuously change between experiments, so it is hard to test in constant test conditions.

| | Individual PV Panels | | | | | Maximum Power Point | | | | | System Performance | |
|---|---|---|---|---|---|---|---|---|---|---|---|---|
| System | $PV_1$ (W) | $PV_2$ (W) | $PV_3$ (W) | $PV_4$ (W) | $PV_{sum}$ (W) | $P_{in}$ (W) | $P_{out}$ (W) | $V_{out}$ (V) | $I_{out}$ (A) | Module efficiency | Tracking efficiency | System efficiency |
| **Outdoor even condition** | | | | | | | | | | | | |
| **Series** | 67.79 | 65.78 | 67.00 | 66.35 | 266.93 | 266.93 | 258.87 | 37.14 | 6.97 | 96.97% | 100% | **96.97%** |
| **Segmented DPP** | 63.70 | 61.08 | 61.14 | 60.08 | 233.06 | 233.06 | 245.19 | 33.39 | 6.98 | 95.05% | 99.66% | **94.74%** |
| **Outdoor uneven condition** | | | | | | | | | | | | |
| **Series** | 50.05 | 63.41 | 63.09 | 62.91 | 239.47 | 202.85 | 197.83 | 44.06 | 4.49 | 97.52% | 84.71% | **82.61%** |
| **Segmented DPP** | 52.02 | 61.42 | 59.32 | 58.62 | 231.38 | 223.23 | 211.45 | 35.96 | 5.88 | 94.72% | 96.48% | **91.38%** |

Table 5.2: Test results under outdoor lighting conditions

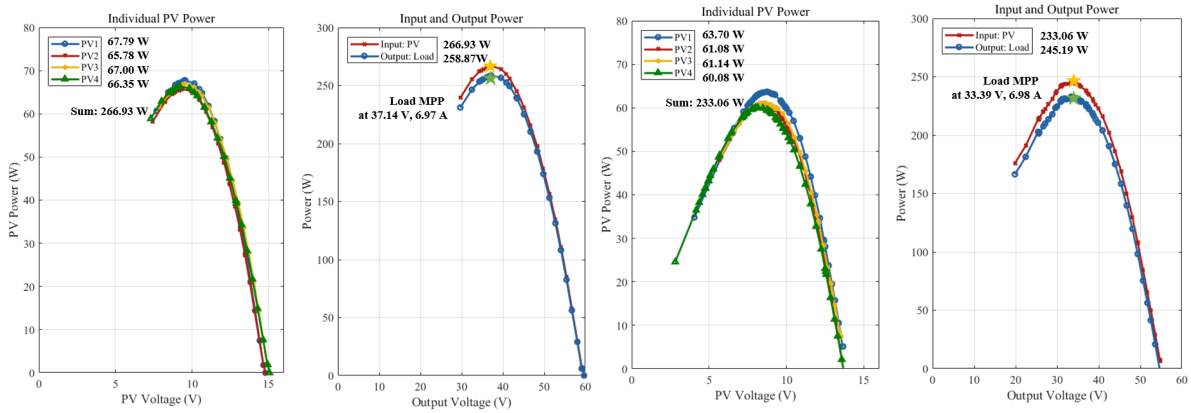


(a) Series-connected system (b) Segmented DPP System

Figure 5.7: P-V curve in even outdoor lighting conditions

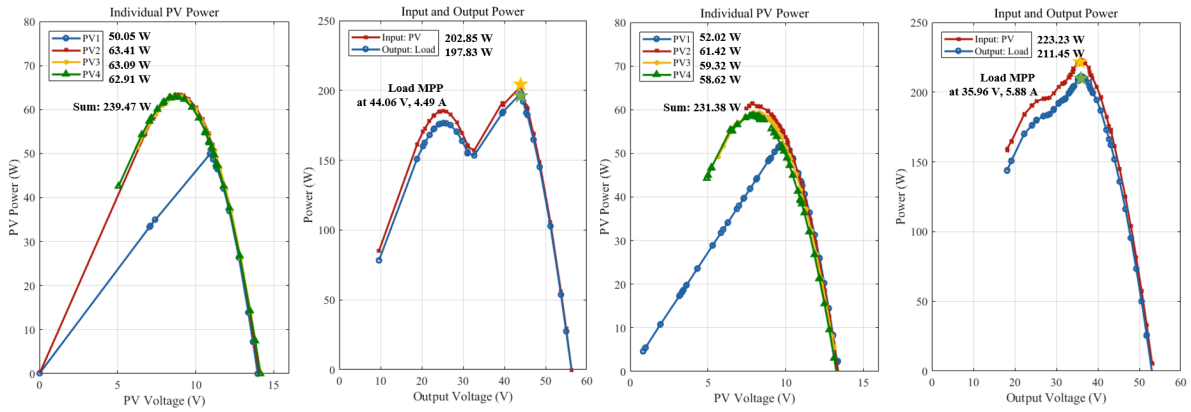


(a) Series-connected system (b) Segmented DPP System

Figure 5.8: P-V curve in uneven outdoor lighting conditions

## 5.3 Indoor Experiment with PV Emulator

As mentioned before, there are limitations on the indoor halogen lamp and outdoor nature sunlight experiment. Therefore, a laboratory PV emulation method was used in indoor experiment, which was introduced and verified in [33]. This PV emulator is simply made with a power source and a PV panel. Figure 5.9 shows the equivalent circuit of a PV cell, which consists of current source, a diode, series and resistance $R_s$ and parallel resistance $R_p$. With this circuit, the output current $I_{PV}$ and voltage $V_{PV}$ can be presented as

$$\begin{aligned} I_{PV} &= I_s - I_d - I_p \\ &= I_s - I_o \left[ \exp\left(\frac{V_d}{V_T}\right) - 1 \right] - \frac{V_d}{R_p} \\ V_{PV} &= V_d - I_{PV} R_s \end{aligned} \tag{9}$$

where $I_s$ is the current generated by light hitting the PV panel, $V_d$ and $I_d$ are the voltage and current through the diode, respectively, and $I_p$ is the current through the parallel resistance. $I_o$ is the reverse saturation current of the diode and $V_T$ is the thermal voltage [34, 35]. Based on this equivalent circuit model, [33] suggested to replace $I_s$ with a external controllable current source. Therefore, as shown in Figure 5.10, the PV emulator can be composed as an external power source operating in current-limit mode and zero $I_s$. The setting of the power source can be done by regulating the current limit as a short-circuit current and setting the voltage limit as the open-circuit voltage of the PV. With this PV emulation method, the segmented DPP system was experimented on with four PV panels and four power sources, as shown in Figure 5.11.

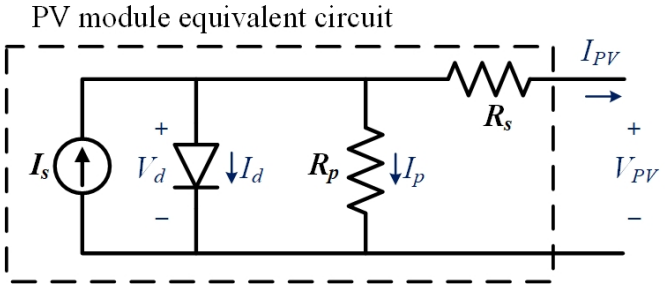


Figure 5.9: Equivalent circuit of the PV module

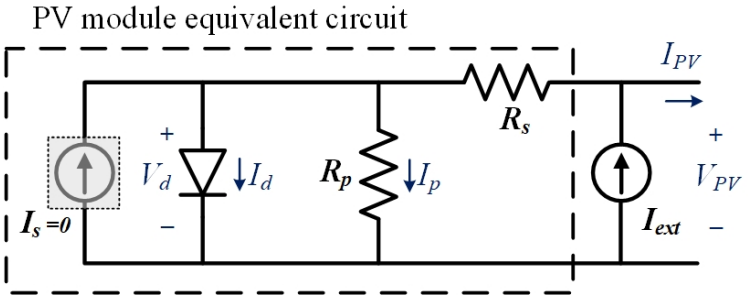


Figure 5.10: Equivalent circuit of the PV module with $I_{ext}$

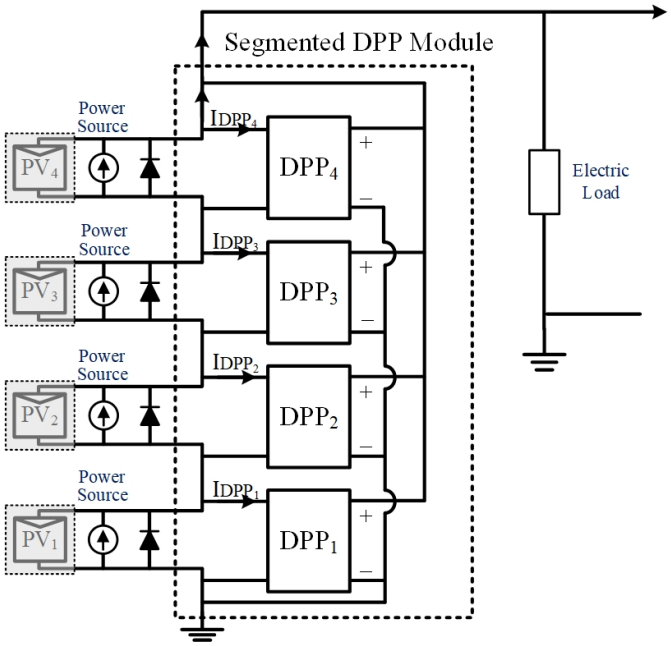


Figure 5.11: Experimental diagram with PV emulator

### 5.3.1 Experimental Results

First, to verify this emulator can be used with the segmented DPP system with realistic PV panel dynamics, four power sources were connected in parrallel to the PV panels, which are completely covered, as shown in Figure 5.12. Figure 5.13 shows the experimental setup and equipment for the segmented DPP system. From left to right, there is an electric load, power analyzers, the hardware prototype, an oscilloscope and four power sources. In this experiment, the power sources were modulated as the amount of the PV output power as in the outdoor experimental condition. Then, the series-connected and the segmented DPP system were tested under both even and uneven lighting cases. Figure 5.14 shows the current flow of DPP converter in uneven lighting.

Figure 5.12: Experimental setup with fully covered PV panel

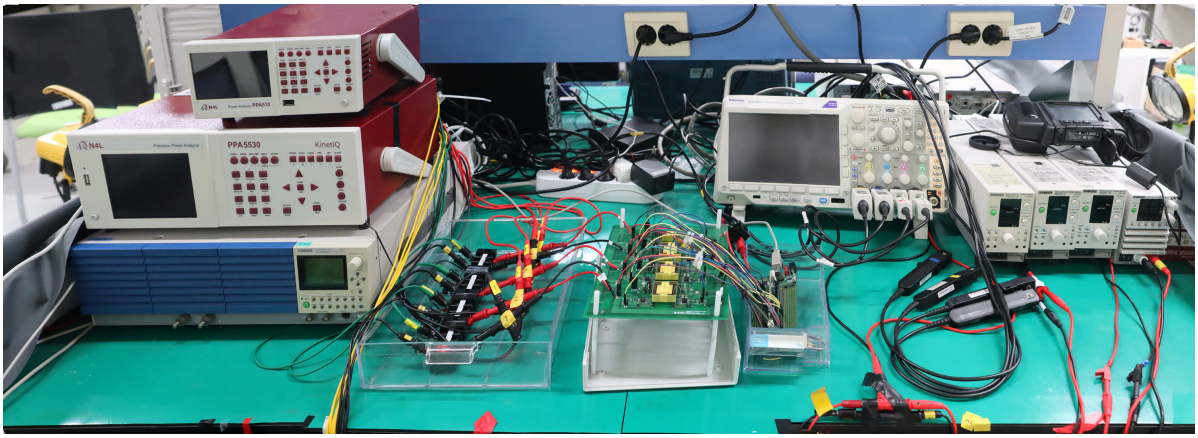

Figure 5.13: Experimental equipment for the segmented DPP system

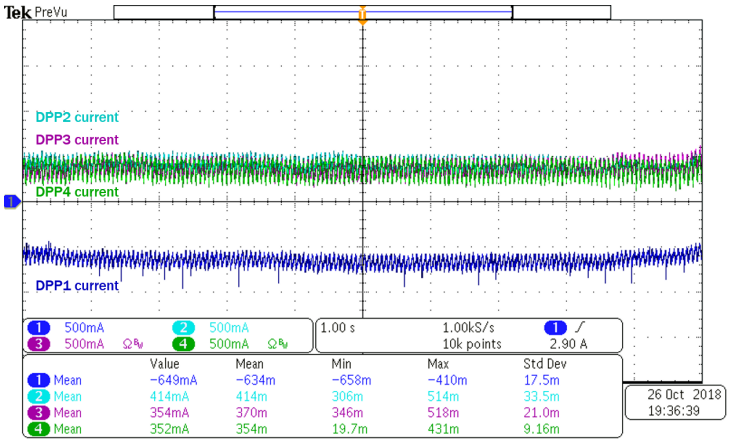


Figure 5.14: Current of DPP converter in uneven lighting condition

The result of two systems under the even lighting case are shown in Figure 5.15, and summarized in Table 5.3. As shown in Figure 5.16, under the uneven lighting case, the segment DPP system has higher output power and system efficiency, which is 94.29%, while the series-connected system efficiency is 88.05%. Also, the string power curve becomes smooth, which has no local MPP. As shown in Figure 5.14, the DPP current, which is connected with the shaded PV flows in the reverse direction and others flow in the forward direction. This means that the segmented DPP converter executes the system algorithm correctly and the PV emulator method can be used for verifying the segmented DPP system in a controlled indoor setting. Therefore, this PV emulator provides more convenient and controllable experimental setup, which can be tested and fairly compared in the same conditions.

| | Individual PV Panels | | | | | Maximum Power Point | | | | | System Performance | |
|---|---|---|---|---|---|---|---|---|---|---|---|---|
| System | $PV_1$ (W) | $PV_2$ (W) | $PV_3$ (W) | $PV_4$ (W) | $PV_{sum}$ (W) | $P_{in}$ (W) | $P_{out}$ (W) | $V_{out}$ (V) | $I_{out}$ (A) | Module efficiency | Tracking efficiency | System efficiency |
| **Indoor emulator even condition** | | | | | | | | | | | | |
| **Series** | 61.99 | 63.03 | 63.42 | 64.67 | 253.12 | 253.12 | 246.41 | 50.11 | 4.91 | 97.35% | 100% | **97.35%** |
| **Segmented DPP** | 63.19 | 62.96 | 63.33 | 63.95 | 253.43 | 252.44 | 241.52 | 51.17 | 4.72 | 95.68% | 99.61% | **95.30%** |
| **Indoor emulator uneven condition** | | | | | | | | | | | | |
| **Series** | 49.83 | 62.80 | 63.38 | 64.56 | 240.58 | 217.07 | 211.83 | 51.54 | 4.11 | 97.59% | 90.23% | **88.05%** |
| **Segmented DPP** | 50.28 | 63.10 | 63.37 | 64.07 | 240.82 | 239.49 | 227.07 | 49.15 | 4.62 | 94.82% | 99.45% | **94.29%** |

Table 5.3: Test results with PV emulator

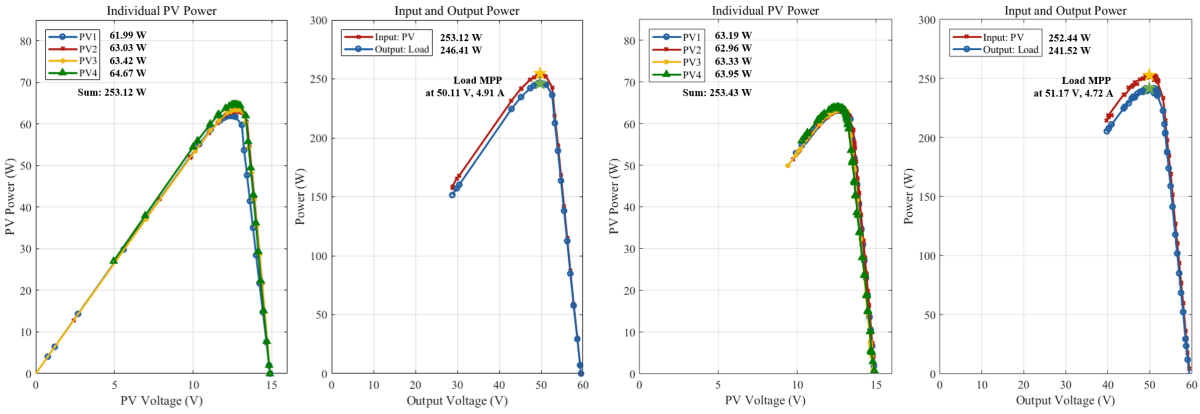


(a) Series-connected system (b) Segmented DPP System

Figure 5.15: P-V curve with indoor emulator in even lighting conditions

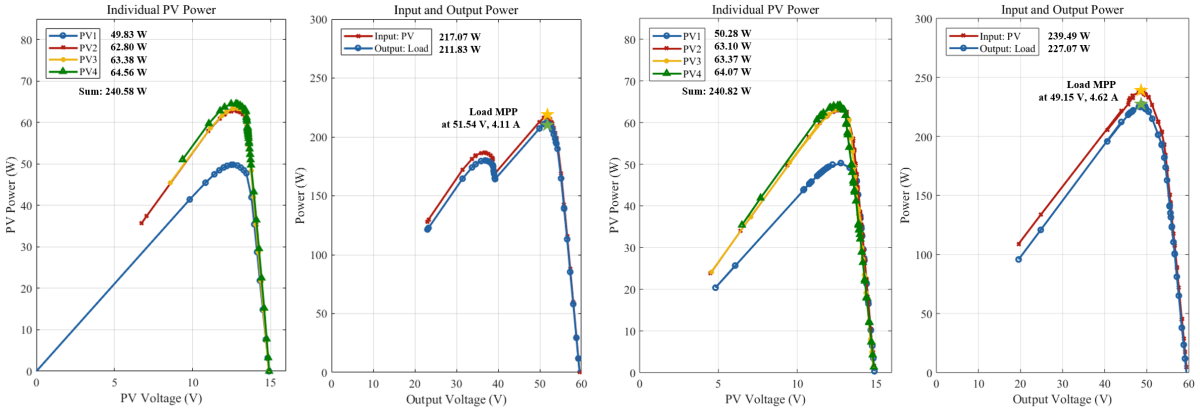


(a) Series-connected system (b) Segmented DPP System

Figure 5.16: P-V curve with indoor emulator in uneven lighting conditions

# VI Optimized Design and Result Analysis

## 6.1 System Optimization

### 6.1.1 Hardware Update

Based on the previous prototype, on updated hardware was developed. First, in the view point of the DPP converter board, the previous version of the DPP converter consisted of four individual flyback converters. Each DPP converter needed one DC-DC converter and two LDOs, four DC-DC converters and eight LDOs in one segmented DPP module. However, if the four flyback converters are implemented in one converter board, then three DC-DC converters and two LDOs are needed in one module, which has fewer components than the previous one. This can reduce the power losses and cost. The comparison diagram of the DPP module is shown in Figure. 6.1. As drawn in this diagram, the wire complexity and loss are reduced by replacing wires with PCB copper layout.

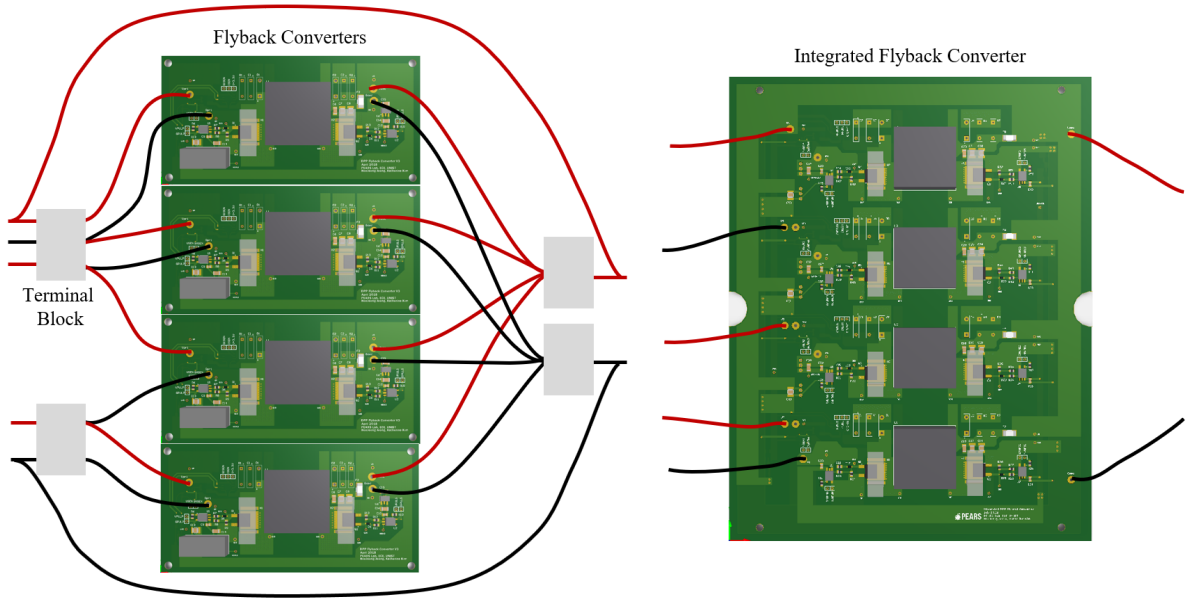


(a) Diagram of previous segmented DPP module (b) Diagram of updated segmented DPP module

Figure 6.1: Comparison of the previous and updated segmented DPP module

Second, to achieve higher module efficiency, the turns number of the coupled inductor was reduced, which reduces conduction loss through the coupled inductor. The parameters of updated flyback converter are shown in Table 6.1. The total turns number of the coupled inductor was reduced from 30 to 26 turns. By reducing this turn number, the efficiency of flyback converter increased to 90.42% in the forward direction and 87.52% in the reverse direction. Figure 6.2 shows the efficiency of one flyback converter according to the input power and the dash line presents the efficiency including the power loss of LDOs and sensors. Compared with the previous converter efficiency, it increased 1.38% in the forward direction (87.75% to 89.10%) and 1.57% in the reverse direction (83.81% to 85.38%).

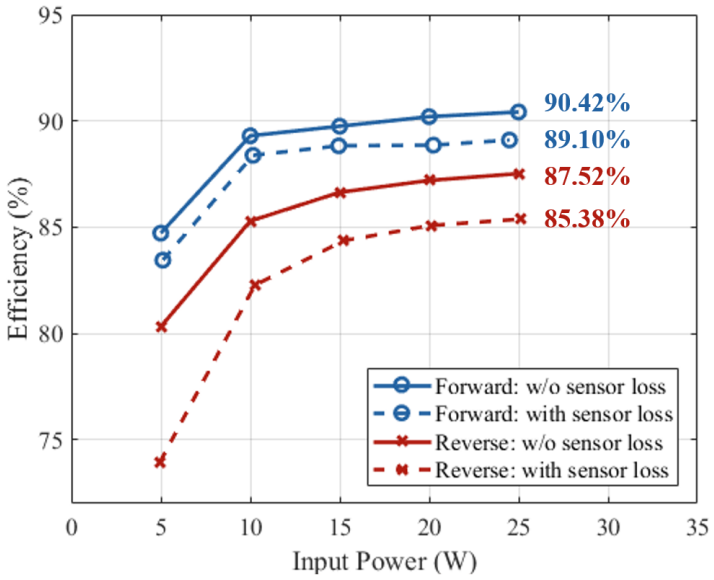


Figure 6.2: Efficiency of updated bidirectional flyback converter

| | | Primary | Secondary |
|---|---|---|---|
| **Power** | **Voltage (V)** | 12.8 | 51.2 |
| | **Current (A)** | 2.0 | 0.5 |
| | **Switching frequency (kHz)** | 100 | |
| **Coupled inductor** | **Turn number** | 7 | 19 |
| | **Magnetizing inductance (μH)** | 8.9 | 64.88 |
| | **Leakage inductance (μH)** | 0.25 | 1.92 |
| **Snubber** | **Capacitance (nF)** | 200 | 10 |
| | **Resistance (Ω)** | 1200 | 2400 |

Table 6.1: Design parameters of updated bidirectional flyback converter

### 6.1.2 Algorithm Update

As shown in the previous testing results, the system efficiency with the segmented DPP module is clearly higher than the series-connected system under the uneven lighting conditions. However, in the even lighting conditions, the system efficiency of the series-connected system has been higher. Because the PV current at MPP is the same for the PV panels in even conditions, the series-connected system also can track the MPP. In this situation, there is only line loss with the series string system, while the segmented DPP system has both line loss and converter loss. Therefore, to minimize this converter loss, the additional function was implemented, which can reduce the switching loss under even lighting conditions. As shown in Figure 6.3, in the case of the previous algorithm code, even the reference current is near zero, the switching signal drives the converter. To eliminate this switching loss, when the reference current is lower than a set value, the converter switching operation turbs off. By adding

this additional function, the switching loss can be removed, and it increases the system efficiency of the segmented DPP system in even lighting conditions.

**Previous code**

```
if (Ireffly1 >= 0)
{
    EPwm1Regs.CMPA.half.CMPA = dfly1;
    EPwm1Regs.CMPB = 0;//
}
else
{
    EPwm1Regs.CMPA.half.CMPA = 0;
    EPwm1Regs.CMPB = dfly1;//
}
```

**Updated code**

```
if (Ireffly1 > 0 + dzero)
{
    EPwm1Regs.CMPA.half.CMPA = dfly1;
    EPwm1Regs.CMPB = 0;//
}
```

Forward direction

```
else if (Ireffly1 < 0 - dzero)
{
    EPwm1Regs.CMPA.half.CMPA = 0;
    EPwm1Regs.CMPB = dfly1;//
}
```

Reverse direction

```
else
{
    EPwm1Regs.CMPA.half.CMPA = 0;
    EPwm1Regs.CMPB = 0;
}
```

Converter off

Figure 6.3: Comparison of the previous and updated algorithm as duty ratio control code

## 6.2 Experimental Results

With the updated design and PCB layout, the segmented DPP module was fabricated and built as shown in Figure 6.4. Also, the updated algorithm was implemented into the TMS320F28335 DSP controller.

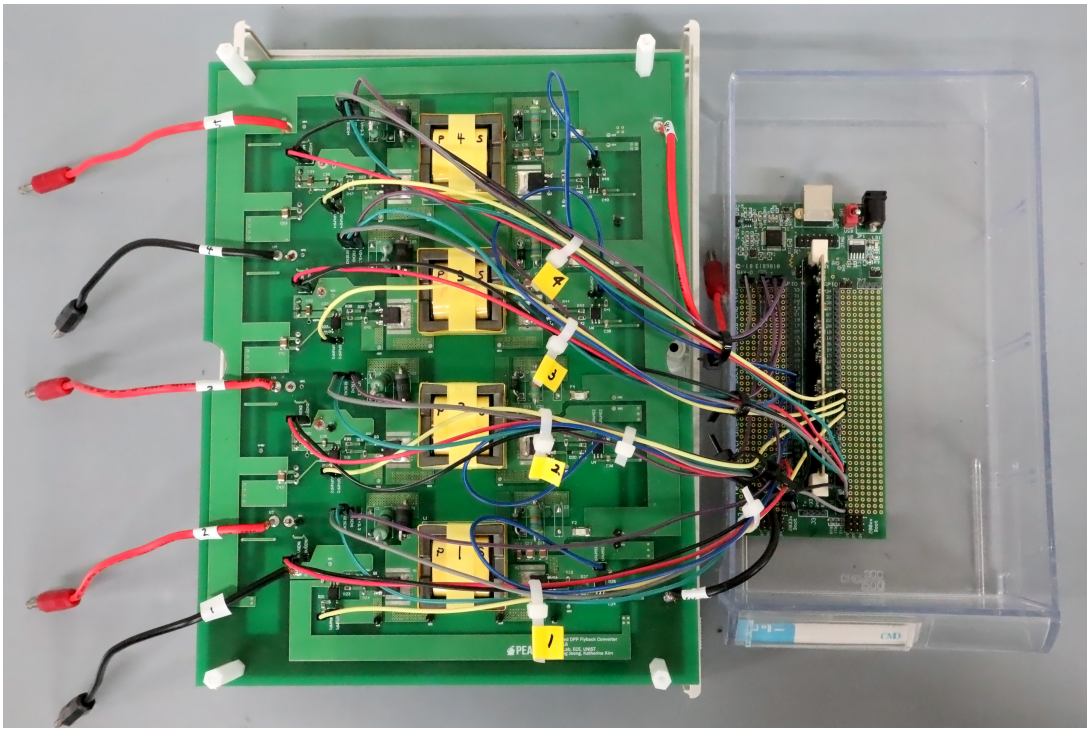

Figure 6.4: Updated segmented DPP module with DSP controller

### 6.2.1 Comparison with Previous Prototype

With the updated prototype and algorithm, the testing was conducted under the same conditions are in Table 5.3 to show the efficiency improvement compared with the previous prototype. The first PV ($PV_1$) was mismatched at 20%. Table 6.2 shows the experimental results, comparing the previous (DPP 1) and the updated prototype (DPP 2) module with indoor PV emulator setup. As shown in the results, the system efficiency using the updated DPP module increased from 95.30% to 96.17%, such that the power loss decreased by 1.5 W. This is because the converter was turned off under even lighting condition, which reduced the switching loss. In Figure 6.5, there is a period where the DPP currents become zero. This displays that the converters are successfully turned off, as the current reference is set near zero. Also, according to Table 6.2, in the uneven conditions, the efficiency of the segmented DPP system was increased about 1%, which is a 1.5 W reduction in loss. This is because of the reduced module loss attribute to decreasing the turns number of the flyback converter and integrating the four flyback converters into one PCB. Figure 6.6 and Figure 6.7 show the power-voltage curves of the updated segmented DPP module under even and uneven lighting conditions. To compare the output power of the updated prototype with the series-connected and previous segmented module, it is helpful to refer the power-voltage curve in Figure 5.15, 5.16, 6.6 and 6.7.

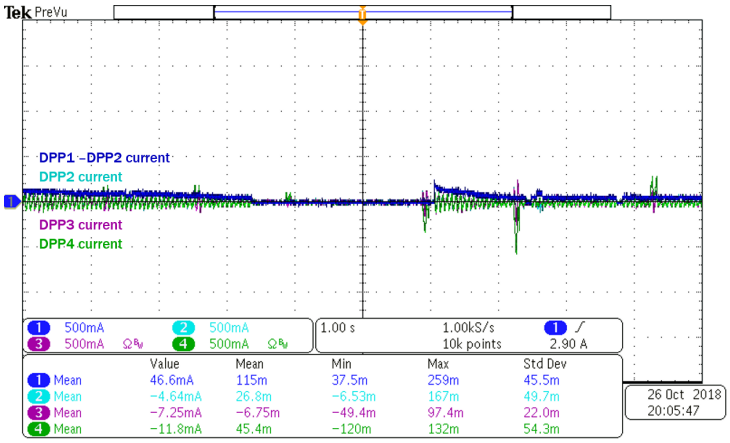


Figure 6.5: Current of DPP converter in even lighting condition

| | Individual PV Panels | | | | | Maximum Power Point | | | | | | System Performance | |
|---|---|---|---|---|---|---|---|---|---|---|---|---|---|
| System | $PV_1$ (W) | $PV_2$ (W) | $PV_3$ (W) | $PV_4$ (W) | $PV_{sum}$ (W) | $P_{in}$ (W) | $P_{out}$ (W) | $V_{out}$ (V) | $I_{out}$ (A) | Module loss (W) | Module efficiency | Tracking efficiency | System efficiency |
| **Indoor emulator even condition** | | | | | | | | | | | | | |
| **Series** | 61.99 | 63.03 | 63.42 | 64.67 | 253.12 | 253.12 | 246.41 | 50.11 | 4.91 | **6.71** | 97.35% | 100% | **97.35%** |
| **DPP 1** | 63.19 | 62.96 | 63.33 | 63.95 | 253.43 | 252.44 | 241.52 | 51.17 | 4.72 | **10.92** | 95.68% | 99.61% | **95.30%** |
| **DPP 2** | 62.86 | 63.00 | 63.48 | 64.94 | 254.28 | 253.92 | 244.54 | 50.11 | 4.88 | **9.38** | 96.31% | 99.86% | **96.17%** |
| **Indoor emulator uneven condition** | | | | | | | | | | | | | |
| **Series** | 49.83 | 62.80 | 63.38 | 64.56 | 240.58 | 217.07 | 211.83 | 51.54 | 4.11 | **5.24** | 97.59% | 90.23% | **88.05%** |
| **DPP 1** | 50.28 | 63.10 | 63.37 | 64.07 | 240.82 | 239.49 | 227.07 | 49.15 | 4.62 | **12.41** | 94.82% | 99.45% | **94.29%** |
| **DPP 2** | 50.39 | 62.81 | 63.05 | 64.61 | 240.85 | 240.31 | 229.44 | 51.10 | 4.49 | **10.87** | 95.48% | 99.78% | **95.26%** |

Table 6.2: Test results of previous (DPP1) and updated segmented DPP module (DPP2)

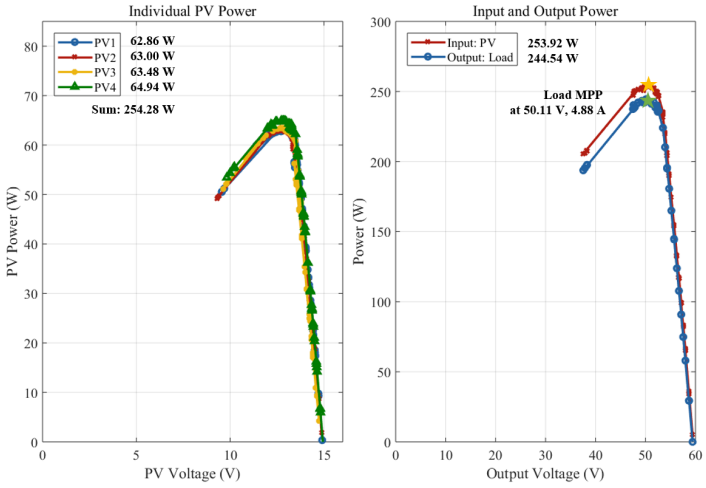


Figure 6.6: P-V curve with indoor emulator in even lighting condition (DPP2)

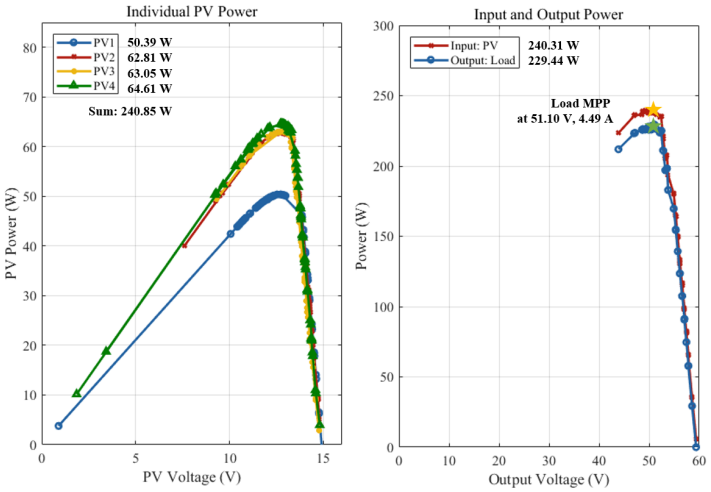


Figure 6.7: P-V curve with indoor emulator in uneven lighting condition (DPP2)

### 6.2.2 Comparison with Different Converter Limits

Normally, the operating voltage of the DPP converter is based on the MPP voltage, so the power rating is proportional to the current rating of the DPP converter. Therefore, to limit the power rating of the bidirectional flyback converter, which was described in Section IV, the converter current is limited through the control algorithm. To compare the MPP tracking efficiency and system efficiency according to the limitation of the converter performance, the current and duty ratio were limited as shown in Table 6.3. In Case A, the segmented DPP converter was limited to 1.5 A current, and 40% duty. The duty limit was increased to 55% in Case B and the current limit was increased to 2 A in Case C. These three cases with segmented DPP system and series-connected system were tested under the condition as shown in Figure 6.8a. The $I_{sc}$ of $PV_1$ is 7 A, and that of $PV_2$ and $PV_3$ are 5 A each, and $PV_4$ is 3 A, which have 2-A current differences.

| | **Duty limit** | **Current limit** |
|---|---|---|
| Case A | 0.4 | ±1.5 A |
| Case B | 0.55 | ±1.5 A |
| Case C | 0.55 | ±2 A |

Table 6.3: Cases of the segmented DPP converter limit

First, as shown in Figure 6.8, the series system has three local maximum and the generated power is 172.93 W, while the ideal maximum power is 237.31 W, which means 57.16 W lower output power than ideal power. Therefore, this system has 75.91% tracking efficiency and results in 72.87% system efficiency. With the segmented DPP system, the ideal tracking efficiency is 100%, which means the converter tracks the maximum power point perfectly. To reach high tracking efficiency, the rated power of the DPP converter is important. If the current difference between the PV panels becomes 2 A, then that much of current should flow through the DPP converters. However, there is a reference current and duty ratio limit on the performance of the converters. For example, in Case A, which limits the duty and current, the tracking efficiency is only 95.34%. To calculate the limited current of the first DPP converter, Equation (3) can be written as

$$I_{sec} = \frac{D_1^2 V_{pri}^2 T}{2 L_{mp} V_{sec}} \tag{10}$$

When solving this equation with the measured current and voltage value and duty ratio ($D_1$) as 0.4, the secondary current ($I_{sec}$) becomes 0.304 A and secondary-side power becomes 15.43 W. Let the converter efficiency be 84.5%, then the primary-side current ($I_{pri}$) becomes 1.18 A. In other words, the 0.4 duty ratio limits the primary-side current to 1.18 A, which is lower than the set 1.5 A current limit. Therefore, to reach the current limit as a set value, a sufficient duty ratio limit is required. When the duty limitation was increased to 0.55, the tracking efficiency became 97.91%, which allowed the current limit to be 1.5 A. When the current limit was increased to 2 A, the tracking efficiency increased to 99.94%, which tracks the maximum power point without reaching the limit. Figure 6.10 shows the DPP current of the converters in Case B and Case C.

| | Individual PV Panels | | | | | Maximum Power Point | | | | | System Performance | |
|---|---|---|---|---|---|---|---|---|---|---|---|---|
| System | $PV_1$ (W) | $PV_2$ (W) | $PV_3$ (W) | $PV_4$ (W) | $PV_{sum}$ (W) | $P_{in}$ (W) | $P_{out}$ (W) | $V_{out}$ (V) | $I_{out}$ (A) | Module efficiency | Tracking efficiency | System efficiency |
| **Series** | 81.75 | 59.20 | 59.60 | 36.77 | 237.31 | 180.15 | 172.93 | 36.33 | 4.76 | 95.99% | 75.91% | **72.87%** |
| **Case A** | 82.07 | 59.33 | 59.42 | 36.94 | 237.76 | 226.69 | 213.32 | 50.67 | 4.21 | 94.10% | 95.34% | **89.72%** |
| **Case B** | 82.05 | 59.27 | 59.31 | 36.87 | 237.51 | 232.55 | 218.33 | 50.19 | 4.35 | 93.88% | 97.91% | **91.92%** |
| **Case C** | 82.30 | 59.43 | 59.44 | 36.96 | 238.13 | 237.99 | 224.44 | 50.21 | 4.47 | 94.31% | 99.94% | **94.25%** |

Table 6.4: Test results with different converter limits

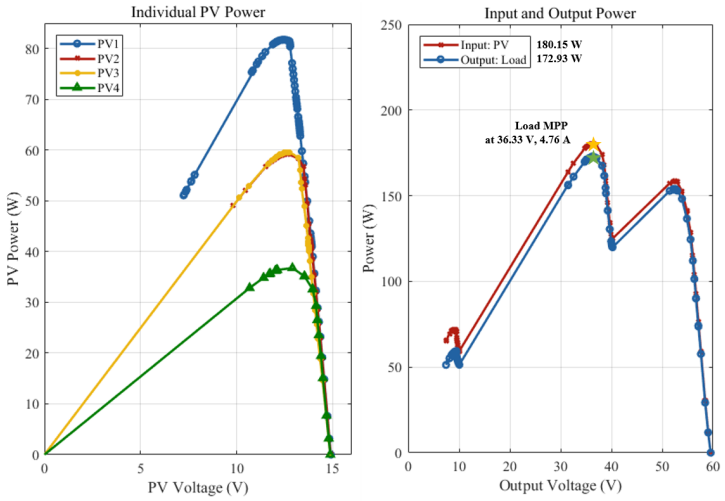


(a) Series-connected system

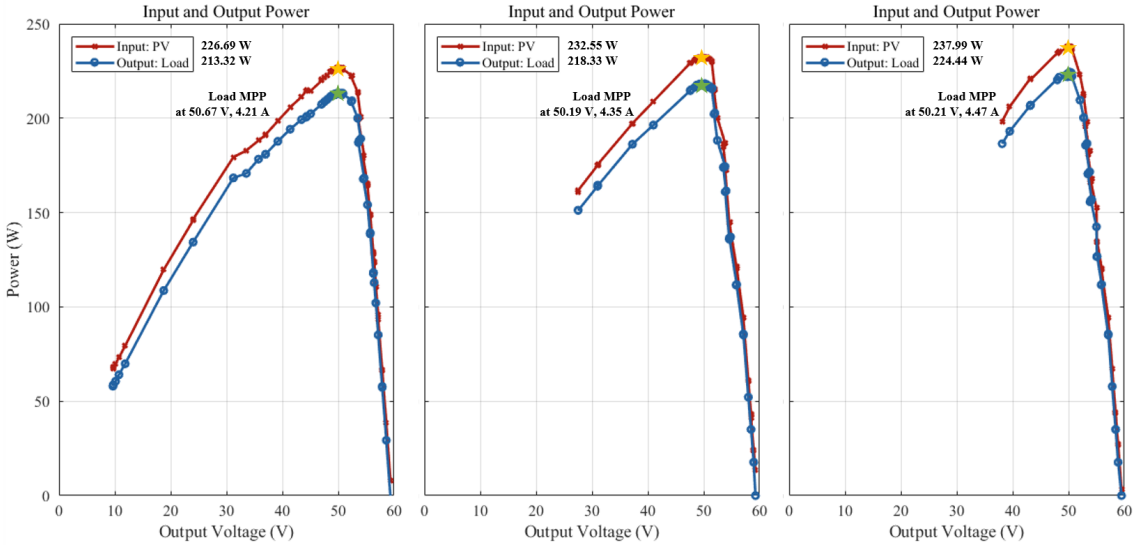


(b) Segmented DPP system with Case A (left), Case B (middle), and Case C (right)

Figure 6.8: P-V curve with different converter limits

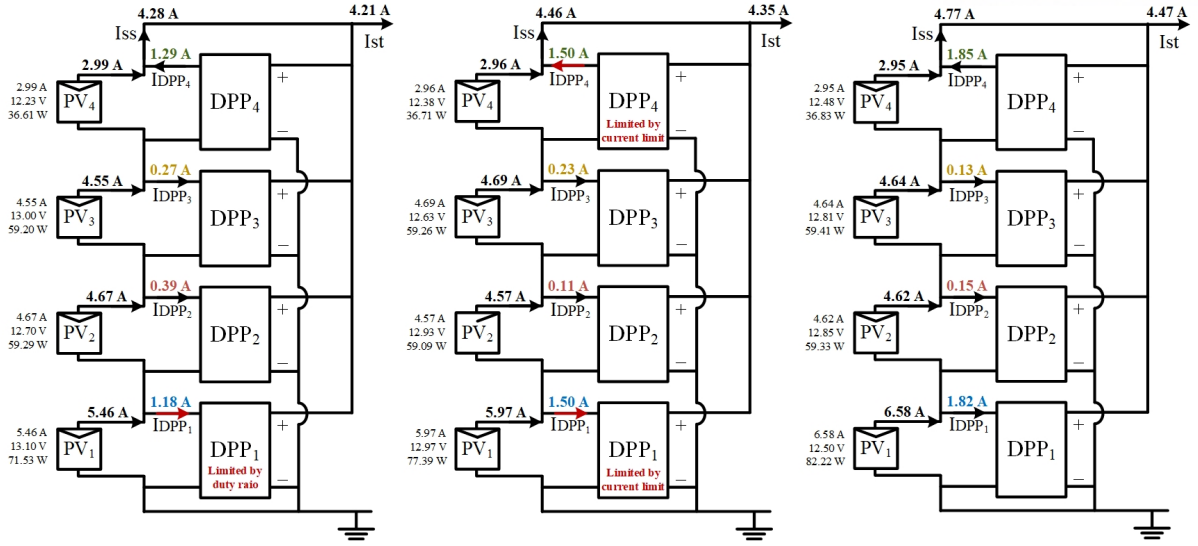


(a) Case A (b) Case B (c) Case C

Figure 6.9: Diagram of the current flow at maximum power point operation

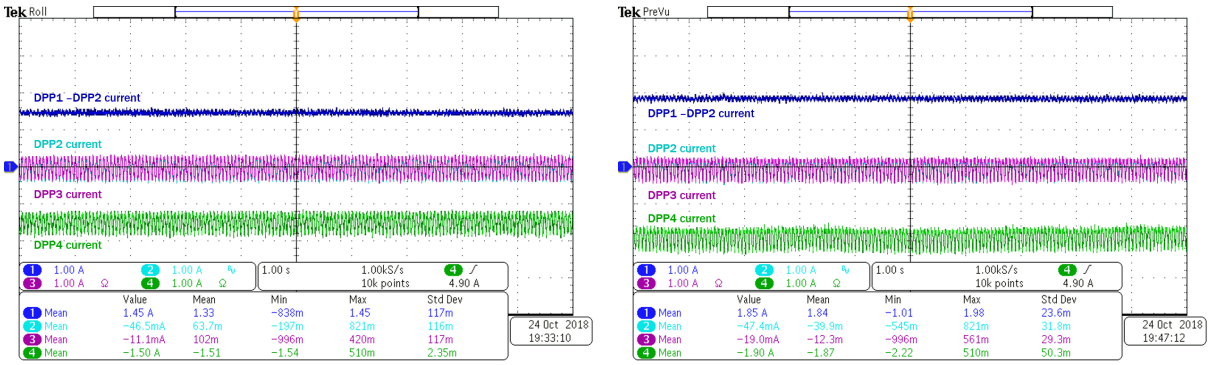


(a) Case B (b) Case C

Figure 6.10: Current of DPP converter with (a) Case B and (b) Case C

### 6.2.3 Comparison of Various Shading Changes

To see how much the segmented DPP converter can compensate for different shading intensity, the experimental setup was set as outlined in Table 6.5. In Case 1, the emulator was set as the four PV panels are in even irradiance, which have same the short-circuit current ($I_{sc}$). From Case 2 to Case 5, $I_{sc}$ of the fourth PV was decreased in intervals of 1 A, and in Case 6, $I_{sc,4}$ was set as 2.5 A, which results in the 64.29% mismatch.

| | $I_{sc,1}$ (A) | $I_{sc,2}$ (A) | $I_{sc,3}$ (A) | $I_{sc,4}$ (A) | Shading (%) |
|---|---|---|---|---|---|
| Case 1 | 7 | 7 | 7 | **7** | 0 |
| Case 2 | 7 | 7 | 7 | **6** | 14.92 |
| Case 3 | 7 | 7 | 7 | **5** | 28.57 |
| Case 4 | 7 | 7 | 7 | **4** | 42.86 |
| Case 5 | 7 | 7 | 7 | **3** | 57.14 |
| Case 6 | 7 | 7 | 7 | **2.5** | 64.29 |

Table 6.5: Cases of the PV shading setup

Figure 6.11a shows the individual PV power of Case 1 to Case 6. As shown in the figure, the maximum power of the fourth PV panel decreases from Case 1 to Case 6, so that the mismatch becomes larger. In Case 1, the series-connected system has the highest system efficiency, which is 97.05%, since four PV panels are in even irradiance conditions. In the case of the segmented DPP system, there is an additional power loss of 2 W compared to the series system. This is because of the additional converter loss from the DPP module. However, from Case 2 where mismatch begins to occur, the efficiency of the segmented system has clearly higher system efficiency than the series-string system. In Case 2, the fourth panel has a mismatch of 14.92% compared to other PV panels. In this case, the MPP tracking efficiency in the series-connected system is reduced to 94.99%, which means that the PV panels are not operating at its MPP. In contrast, the tracking efficiency of the segmented DPP system is still 99.57%, which means that the PV panels are operating at its maximum power point. Therefore, in the segmented DPP system, the system efficiency was increased by 3% and output power was increased by 10 W compared with the series-connected system. As mismatch becomes more severe, differences between system efficiency also becomes larger due to the MPP tracking performance between the two systems.

In the series-connected system with Case 1 to Case 3, the voltage at MPP is the same as the sum of four PV voltages. However, as the mismatch increases, Case 4 has MPP voltage at the sum of three PV voltages. At this point, only three PVs ($PV_1, PV_2, PV_3$) were used to make the maximum power point, so Case 4 to Case 6 has the same maximum power. While the total power of the PV panel is decreasing, the maximum power of the series system has a constant power after a certain shading level. Due to this situation, the tracking efficiency actually increased in series-connected system.

The segmented DPP system maintains the tracking efficiency over 99%, which follows the real

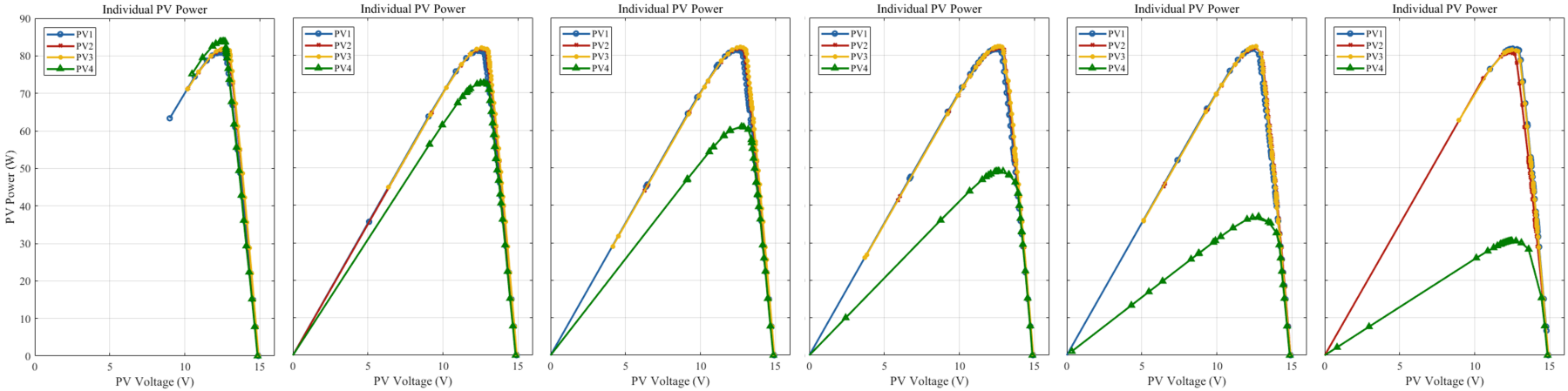


(a) Individual PV power from Case 1 (left) to Case 6 (right)

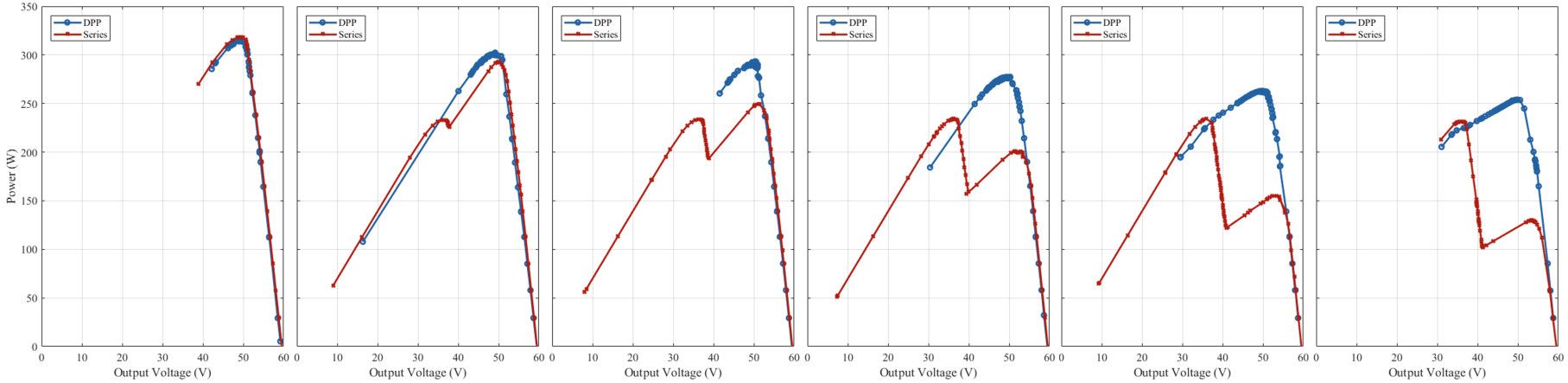


(b) Output power of the series-connected (red) and segmented DPP system (blue) under Case 1 (left) to Case 6 (right)

Figure 6.11: P-V curves according to shading changes

maximum power point of each PV panel. As the mismatch increases, the current flowing through the converter becomes larger, which results in higher power loss through the converter, which decreases the system efficiency. Despite of this converter loss, the segmented DPP system has higher system efficiency than the series-connected system in the uneven lighting condition, because the PV panels are following the maximum power point. The segmented DPP system has maximum 14.8% higher system efficiency and 43.3 W higher output power, as shown in Figure 6.12.

| | **Individual PV Panels** | | | | | **Segmented DPP Module** | | | | | | **System Performance** | |
|---|---|---|---|---|---|---|---|---|---|---|---|---|---|
| System | $PV_1$ (W) | $PV_2$ (W) | $PV_3$ (W) | $PV_4$ (W) | $PV_{sum}$ (W) | $P_{in}$ (W) | $P_{out}$ (W) | $V_{out}$ (V) | $I_{out}$ (A) | Module loss (W) | Module efficiency | Tracking efficiency | System efficiency |
| **Series-connected system** | | | | | | | | | | | | | |
| **Case 1** | 80.87 | 81.57 | 81.81 | 83.84 | 328.09 | 328.07 | 318.41 | 49.29 | 6.46 | 9.66 | 97.06% | 99.99% | **97.05%** |
| **Case 2** | 81.12 | 81.67 | 81.94 | 72.58 | 317.30 | 301.39 | 292.80 | 49.88 | 5.87 | 8.60 | 97.15% | 94.99% | **92.28%** |
| **Case 3** | 81.35 | 81.79 | 82.11 | 60.95 | 306.20 | 256.48 | 249.73 | 51.07 | 4.89 | 6.75 | 97.37% | 83.76% | **81.56%** |
| **Case 4** | 81.59 | 81.94 | 82.31 | 49.10 | 294.94 | 242.67 | 234.16 | 36.36 | 6.44 | 8.51 | 96.49% | 82.28% | **79.39%** |
| **Case 5** | 81.65 | 82.06 | 82.42 | 36.98 | 283.12 | 243.76 | 234.49 | 36.02 | 6.51 | 9.27 | 96.20% | 86.10% | **82.82%** |
| **Case 6** | 81.75 | 80.64 | 81.46 | 30.47 | 274.32 | 241.68 | 231.37 | 35.65 | 6.49 | 10.31 | 95.73% | 88.10% | **84.34%** |
| **Segmented DPP system** | | | | | | | | | | | | | |
| **Case 1** | 80.74 | 81.39 | 81.52 | 83.34 | 326.99 | 326.79 | 315.14 | 49.24 | 6.40 | 11.65 | 96.43% | 99.94% | **96.38%** |
| **Case 2** | 81.50 | 82.12 | 81.64 | 72.40 | 317.65 | 316.28 | 302.33 | 49.16 | 6.15 | 13.94 | 95.59% | 99.57% | **95.18%** |
| **Case 3** | 81.86 | 82.01 | 82.15 | 61.00 | 307.01 | 306.52 | 293.42 | 50.33 | 5.83 | 13.10 | 95.73% | 99.84% | **95.57%** |
| **Case 4** | 81.72 | 81.59 | 82.14 | 49.12 | 294.57 | 293.97 | 277.44 | 50.26 | 5.52 | 16.53 | 94.38% | 99.80% | **94.18%** |
| **Case 5** | 81.83 | 81.86 | 81.54 | 36.96 | 282.19 | 281.69 | 263.04 | 49.63 | 5.30 | 18.65 | 93.63% | 99.55% | **93.21%** |
| **Case 6** | 81.26 | 80.98 | 81.32 | 30.49 | 274.04 | 273.13 | 254.04 | 49.91 | 5.09 | 19.08 | 93.01% | 99.66% | **92.70%** |

Table 6.6: Test results according to the shading changes

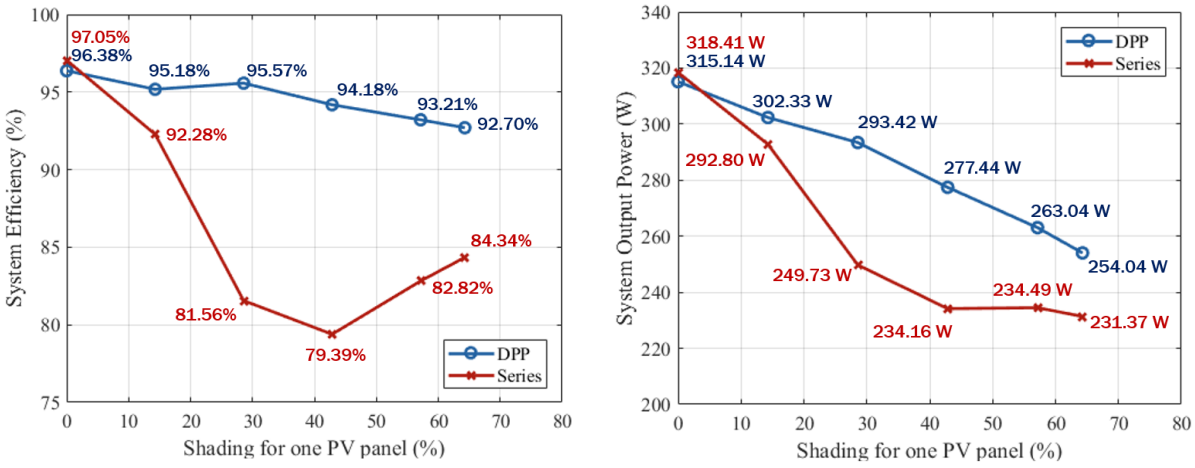


(a) System efficiency

(b) System output power

Figure 6.12: (a) System efficiency and (b) system output power according to shading on PV panel

### 6.2.4 Operation with Inverter MPPT

To test the segmented system with real inverter MPPT operation, the electric load was used to emulate an inverter using Python code. The electric load controls the string current according to a P&O algorithm and makes the output track the MPP. The condition of the PVs are shown in Figure 6.13a, where two PVs are realtively high power and two PVs are low power. As shown in Figure 6.14, the output power of the series-connected system has 242 W at steady-state, however, the segmented DPP system has 269 W power, which is higher than the series-connected system and tracks the MPP of each PV panel.

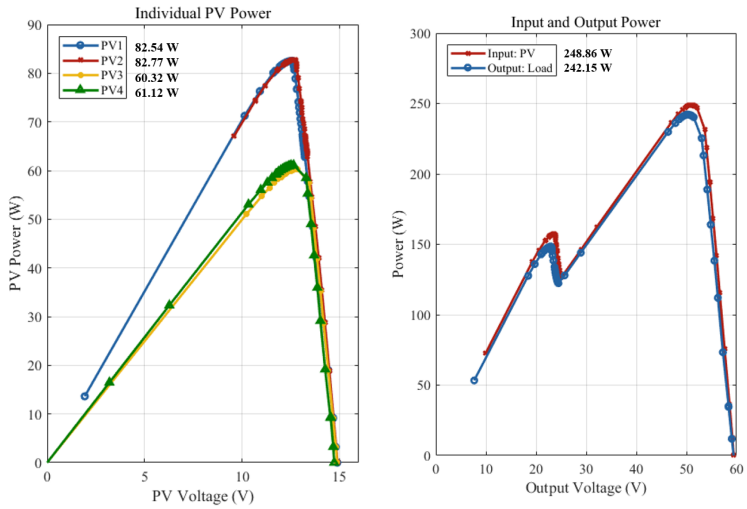


(a) (b)

Figure 6.13: P-V curves for (a) individual PV power and (b) output power of series connected system

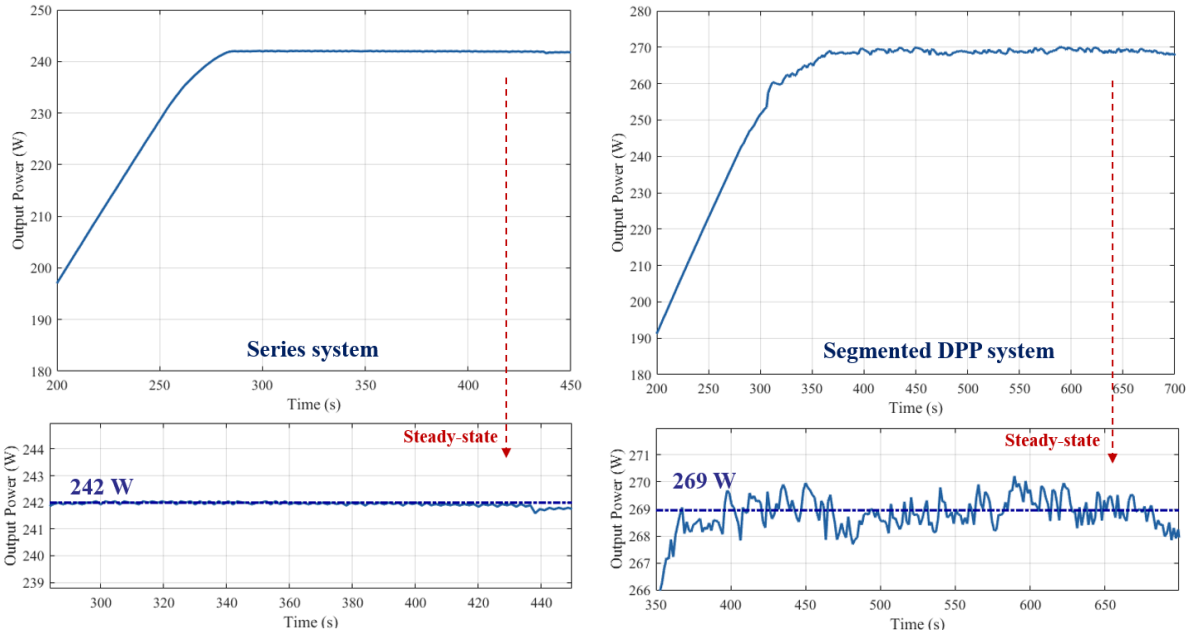


(a) Series-connected system (b) Segmented DPP system

Figure 6.14: Experimental results with inverter MPPT operation

# VII Conclusion

This work introduced the segmented DPP system architecture, which is a modified structure of the PV-to-bus DPP architecture that addresses scalability and modularity problems of previous systems. The proposed structure can achieve higher system efficiency compared to conventional PV systems in uneven lighting conditions. Also, the modular approach of the segmented DPP system allows for lower voltage ratings of the converters, simpler wire connections, ease-of-installation, and scalability compared to the conventional DPP converter system. For this work, $n = 4$ PV panels were connect to one segmented DPP module, which contained four bidirectional flyback DPP converters. To control the converters, a segmented DPP module algorithm was proposed that utilized voltage balance and MPPT modes to achieve individual MPPT of each PV panel.

The operation of this system and control algorithm was implemented in Matlab/Simulink simulation, which verified the convergence to the MPP. An experimental prototype was also developed and tested using an indoor and outdoor testing setup. Also, PV emulator method was used to test the system in a controllable lighting condition. Under uneven lighting conditions, the segmented DPP system consistently increased the output power compared to series connection and created a convex power curve at the output. With the segmented DPP module, the system efficiency was 95.30% under even lighting and 94.29% under uneven lighting. In addition, the converter design and control algorithm were improved by reducing the converter losses. With this updated converter, the converter module loss was decreased by about 1.5 W. This updated segmented DPP system was tested in various lighting conditions using the PV emulator setup. The performance limit of the DPP converters were increased to improve tracking efficiency in mismatched conditions. When there is shading on one panel among the four panels, the segmented DPP module increased the system efficiency up to 14.8% compared to the series connection, which is 43.3 W difference at 42.86% mismatch.

## 7.1 Future Work

The segmented DPP system can be improved further by minimizing the cost and size of the design, which results in better performance versus the cost. In terms of the control algorithm, if the segmented DPP algorithm can find a condition of lower loss through the converters, then the module can always operate at an optimal condition. This can increase the module efficiency and decrease the power losses at MPP.

The experimental testing done in the thesis was limited to one module connected to four PV panels. Therefore, to verify this structure in a large-scale systems, at least two segmented DPP modules are needed. Also, this segmented DPP system can be installed with a real inverter connected to the grid.

# References

[1] W. E. Council, "World Energy Resources 2013," World Energy Council, Tech. Rep., 2013.

[2] ——, "World Energy Resources 2016," World Energy Council, Tech. Rep., 2016.

[3] G. A. C. on Global Change (WBGU), *World in Transition: Towards Sustainable Energy Systems*. Earthscan, 2003.

[4] Solargis, "Solar resource: PV power potential maps and GIS data," 2017. [Online]. Available: https://solargis.com

[5] K. A. Kim and P. T. Krein, "Reexamination of Photovoltaic Hot Spotting to Show Inadequacy of the Bypass Diode," *IEEE Journal of Photovoltaics*, vol. 5, no. 5, pp. 1435–1441, Sept 2015.

[6] P. Manganiello, M. Balato, and M. Vitelli, "A Survey on Mismatching and Aging of PV Modules: The Closed Loop," *IEEE Transactions on Industrial Electronics*, vol. 62, no. 11, pp. 7276–7286, Nov 2015.

[7] E. L. Meyer and E. E. van Dyk, "Assessing the reliability and degradation of photovoltaic module performance parameters," *IEEE Transactions on Reliability*, vol. 53, no. 1, pp. 83–92, March 2004.

[8] C. Olalla, C. Deline, D. Clement, Y. Levron, M. Rodriguez, and D. Maksimovic, "Performance of Power-Limited Differential Power Processing Architectures in Mismatched PV Systems," *IEEE Transactions on Power Electronics*, vol. 30, no. 2, pp. 618–631, Feb 2015.

[9] S. Chen, T. Liang, and K. Hu, "Design, Analysis, and Implementation of Solar Power Optimizer for DC Distribution System," *IEEE Transactions on Power Electronics*, vol. 28, no. 4, pp. 1764–1772, April 2013.

[10] Q. Li and P. Wolfs, "A review of the single phase photovoltaic module integrated converter topologies with three different dc link configurations," *IEEE Transactions on Power Electronics*, vol. 23, no. 3, pp. 1320–1333, May 2008.

[11] G. R. Walker and P. C. Sernia, "Cascaded DC-DC converter connection of photovoltaic modules," *IEEE Transactions on Power Electronics*, vol. 19, no. 4, pp. 1130–1139, July 2004.

[12] R. C. N. Pilawa-Podgurski and D. J. Perreault, "Submodule Integrated Distributed Maximum Power Point Tracking for Solar Photovoltaic Applications," *IEEE Transactions on Power Electronics*, vol. 28, no. 6, pp. 2957–2967, June 2013.

[13] T. Shimizu, M. Hirakata, T. Kamezawa, and H. Watanabe, "Generation control circuit for photovoltaic modules," *IEEE Transactions on Power Electronics*, vol. 16, no. 3, pp. 293–300, May 2001.

[14] P. S. Shenoy, K. A. Kim, B. B. Johnson, and P. T. Krein, "Differential Power Processing for Increased Energy Production and Reliability of Photovoltaic Systems," *IEEE Transactions on Power Electronics*, vol. 28, no. 6, pp. 2968–2979, June 2013.

[15] Y. T. Jeon, H. Lee, K. A. Kim, and J. H. Park, "Least Power Point Tracking Method for Photovoltaic Differential Power Processing Systems," *IEEE Transactions on Power Electronics*, vol. 32, no. 3, pp. 1941–1951, March 2017.

[16] M. Uno and A. Kukita, "Two-Switch Voltage Equalizer Using an LLC Resonant Inverter and Voltage Multiplier for Partially Shaded Series-Connected Photovoltaic Modules," *IEEE Transactions on Industry Applications*, vol. 51, no. 2, pp. 1587–1601, March 2015.

[17] ——, "Current Sensorless Equalization Strategy for a Single-Switch Voltage Equalizer Using Multistacked Buck-Boost Converters for Photovoltaic Modules Under Partial Shading," *IEEE Transactions on Industry Applications*, vol. 53, no. 1, pp. 420–429, Jan 2017.

[18] J. Biswas, A. K. M, A. K. G., and M. Barai, "Design, Architecture and Real Time Distributed Coordination DMPPT Algorithm for PV Systems," *IEEE Journal of Emerging and Selected Topics in Power Electronics*, vol. 6, no. 3, pp. 1418–1433, Sept 2018.

[19] H. Jeong, H. Lee, Y. Liu, and K. A. Kim, "Review of Differential Power Processing Converters Techniques for Photovoltaic Applications," *IEEE Transactions on Energy Conversion*, pp. 1–1, 2018.

[20] H. Jeong, H. Cho, T. Kim, Y. Liu, and K. A. Kim, "A Scalable Unit Differential Power Processing System Design for Photovoltaic Applications," in *2018 IEEE 19th Workshop on Control and Modeling for Power Electronics (COMPEL)*, Padova, Italy, June 2018, pp. 1–8.

[21] POSCO, "POSCO Smart data center with the 'QR code' shaped BIPV," 2018. [Online]. Available: https://newsroom.posco.com/kr

[22] L. F. L. Villa, T. Ho, J. Crebier, and B. Raison, "A Power Electronics Equalizer Application for Partially Shaded Photovoltaic Modules," *IEEE Transactions on Industrial Electronics*, vol. 60, no. 3, pp. 1179–1190, March 2013.

[23] G. Chu, H. Wen, L. Jiang, Y. Hu, and X. Li, "Bidirectional flyback based isolated-port submodule differential power processing optimizer for photovoltaic applications," *Solar Energy*, vol. 158, pp. 929 – 940, 2017.

[24] T. Esram and P. L. Chapman, "Comparison of Photovoltaic Array Maximum Power Point Tracking Techniques," *IEEE Transactions on Energy Conversion*, vol. 22, no. 2, pp. 439–449, June 2007.

[25] J. Ahmed and Z. Salam, "An improved perturb and observe (P&O) maximum power point tracking (MPPT) algorithm for higher efficiency," *Applied Energy*, vol. 150, no. 4, pp. 97–108, July 2015.

[26] J. Kwon, K. Nam, and B. Kwon, "Photovoltaic Power Conditioning System With Line Connection," *IEEE Transactions on Industrial Electronics*, vol. 53, no. 4, pp. 1048–1054, June 2006.

[27] C. Olalla, D. Clement, M. Rodriguez, and D. Maksimovic, "Architectures and Control of Submodule Integrated DC–DC Converters for Photovoltaic Applications," *IEEE Transactions on Power Electronics*, vol. 28, no. 6, pp. 2980–2997, June 2013.

[28] R. Bell and R. C. N. Pilawa-Podgurski, "Decoupled and Distributed Maximum Power Point Tracking of Series-Connected Photovoltaic Submodules Using Differential Power Processing," *IEEE Journal of Emerging and Selected Topics in Power Electronics*, vol. 3, no. 4, pp. 881–891, Dec 2015.

[29] S. Park, M. Kim, and J. Jung, "Design Consideration of Bidirectional Flyback Converter for PV Differential Power Processing Modules," in *2018 The Korean Institute of Power Electronics (KIPE) Conference*, July 2018, pp. 135–137.

[30] S. Park, M. Kim, H. Jeong, T. Kim, K. A. Kim, and J. Jung, "Bidirectional Flyback Converter Design Methodology for Differential Power Processing Modules in PV Applications," *The Transactions of The Korean Institute of Power Electronics*, pp. 1–8, 2019.

[31] D. W. Hart, *Power Electronics*. Mc Graw-Hill, 2011, ch. 7, pp. 267–277.

[32] K. A. Kim, P. S. Shenoy, and P. T. Krein, "Converter Rating Analysis for Photovoltaic Differential Power Processing Systems," *IEEE Transactions on Power Electronics*, vol. 30, no. 4, pp. 1987–1997, April 2015.

[33] S. Qin, K. A. Kim, and R. C. N. Pilawa-Podgurski, "Laboratory emulation of a photovoltaic module for controllable insolation and realistic dynamic performance," in *2013 IEEE Power and Energy Conference at Illinois (PECI)*, Feb 2013, pp. 23–29.

[34] M. G. Villalva, J. R. Gazoli, and E. R. Filho, "Comprehensive Approach to Modeling and Simulation of Photovoltaic Arrays," *IEEE Transactions on Power Electronics*, vol. 24, no. 5, pp. 1198–1208, May 2009.

[35] M. A. El-Sharkawi, *Electric Energy: An Introduction, 3rd Edition*. CRC Press, 2013, ch. 6, pp. 109–125.

# Acknowledgements

This research was supported in part by the MSIT (Ministry of Science and ICT), Korea, under the ITRC (Information Technology Research Center) support program (IITP-2017-2017-0-01635) supervised by the IITP (Institute for Information & communications Technology Promotion), and the Research Institute of Industrial Science and Technology (RIST), Korea, through the grant on DPP Technique Development for Improving PV Efficiency (2017A032), and the Basic Science Research Program through the National Research Foundation of Korea (NRF) funded by the Ministry of Education (2016R1D1A1B03931573). This material is based upon work supported by the research funding from Ulsan National Institute of Science and Technology (Grant No. 1.180061.01).

Firstly, I would like to express my sincere gratitude to my advisor Prof. Katherine A. Kim, for her support, guidance and encouragement through my study at UNIST. She always encourage me to find my own motivation and assist with technical advices. Also, I sincerely thank to Prof. Jee-Hoon Jung and Prof. Jun Moon for advising the research method as a researcher.

I would also like to thank all PEARS lab members who are going the same paths together. I would like to wish that they can reach their own goals. Especially, I thank to Jueun Jung and Seungbin Park for their help and support through this project. Without them, the experiment would have been a rough and long journey. I would like to give special thank to all my college friends who always encourage me and give unforgettable memories. Their passion and encouragement makes me to be here. Finally, my deepest appreciation goes to my family for all their support, love, patience, and trust over the years. I could have no gotten here without my parents and sister.